



Revision of the *Chironius bicarinatus* complex (Serpentes: Colubridae): Redefined species boundaries and description of a new species

Vinícius Sudré¹, Albedi Andrade-Junior¹, Manuella Folly¹, Josué A. R. Azevedo², Robson Waldemar Ávila³, Felipe Franco Curcio⁴, Pedro M. Sales Nunes⁵, Paulo Passos¹

1 Departamento de Vertebrados, Museu Nacional, Universidade Federal do Rio de Janeiro, Quinta da Boa Vista, 20940-040, São Cristóvão, Rio de Janeiro, Brazil

2 Coordenação de Biodiversidade, Programa de Coleções Científicas Biológicas, Instituto Nacional de Pesquisas da Amazônia, Manaus, Amazonas, Brazil

3 Departamento de Biologia, Universidade Federal do Ceará, Campus do Pici, Bloco 906, Av. Mister Hull, 60440-900, Fortaleza, Ceará, Brazil

4 Departamento de Biologia e Zoologia, Instituto de Biociências, Universidade Federal de Mato Grosso, Av. Fernando Corrêa da Costa, 2367, 78060-900, Cuiabá, Mato Grosso, Brazil

5 Departamento de Zoologia, Centro de Biociências, Universidade Federal de Pernambuco, Av. Professor Moraes Rego, 1235, Cidade Universitária, 50670-901, Recife, Pernambuco, Brazil

<http://zoobank.org/D576F215-864F-4961-BA1E-01824BB54B36>

Corresponding author: Vinícius Sudré (viniciussudre@gmail.com)

Academic editor Uwe Fritz

Received 12 May 2023

Accepted 7 December 2023

Published 23 January 2024

Citation: Sudré V, Andrade-Junior A, Folly M, Azevedo JAR, Ávila RW, Curcio FF, Nunes PMS, Passos P (2024) Revision of the *Chironius bicarinatus* complex (Serpentes: Colubridae): Redefined species boundaries and description of a new species. *Vertebrate Zoology* 74 85–120. <https://doi.org/10.3897/vz.74.e106238>

Abstract

Currently, the proposed diagnoses for the *Chironius bicarinatus* complex reflect a wide variation in color pattern and pholidosis. Herein, we review the *Chironius bicarinatus* complex based on morphological and molecular data from a sample of 485 specimens covering the species distribution. Our results corroborate the recognition of *C. bicarinatus* and *C. gouveai*, and diagnose a distinct lineage without an available name. Thus, here we describe this new species restricted to the Baturité Massif, a relictual rainforest isolated in the Caatinga xerophytic domain, in the state of Ceará, northeastern Brazil. The new species can be distinguished from its congeners by its unique combination of qualitative and quantitative morphological characters (scale counts, morphometric, color pattern), and is also supported by molecular and ecological evidence. Additionally, we rectify data on the distribution and morphological variability of *C. gouveai* to accurately infer the boundaries between this taxon and *C. bicarinatus*, which was not properly addressed. Finally, we discuss our results in the light of previous studies that suggest diversification hypotheses in the Atlantic Forest already detected for other taxa, highlighting the importance of conserving the areas of “Brejos de Altitude”, in northeastern Brazil, and the southern limit of Serra do Mar up to Serra do Tabuleiro, in southern Brazil.

Keywords

Brejos de Altitude, ecological niche modeling, geographical variation, hemipenial morphology, integrative taxonomy, molecular phylogeny, osteology, species delimitation

Introduction

The snake genus *Chironius* Fitzinger, 1826 currently comprises 23 species of mostly terrestrial and semi-arboreal colubrid snakes that are widespread across Central and South America, ranging from northern Honduras to northeastern Argentina and northwestern Uruguay (Dixon et al. 1993; Uetz et al. 2023). Among all Neotropical colubrid genera, *Chironius* is unique in its presentation of 10 or 12 dorsal scale rows on the midbody, a feature that, combined with other morphological characters and molecular evidence, supports the monophyly of the genus (Hollis 2006; Klaczko et al. 2014; Hamdan et al. 2017; Torres-Carvajal et al. 2019a). The systematics of *Chironius* was approached by Dixon et al. (1993), who revised the taxonomy of the genus and Hollis (2006), who performed a phylogenetic study using Dixon's morphological dataset. Hollis (2006) was the first to find support for the monophyly of the genus and also proposed the elevation of all subspecies recognized by Dixon et al. (1993) to full species status. More recently, Klaczko et al. (2014), Hamdan et al. (2017), and Torres-Carvajal et al. (2019a) proposed phylogenetic hypotheses for the genus *Chironius*, using molecular characters or by combining molecular and morphological characters. Although different authors corroborate the monophyly of the genus, the phylogenetic relationships within *Chironius* still require investigation (see Hamdan et al. 2017; Torres-Carvajal et al. 2019a).

Chironius bicarinatus is widely distributed throughout the Atlantic Forest and northern Pampas, from northeastern to southern regions of Brazil, northeastern Argentina, eastern Paraguay, as well as some records in northwestern Uruguay; inhabiting the coastal tropical forests, semideciduous forests, grasslands and the Araucaria Forest formations (Dixon et al. 1993). Wied (1820) first described *Coluber bicarinatus* based on a male specimen collected near a lake, approximately five leagues from the south bank of the Jucú River, state of Espírito Santo, Brazil (Wied 1820: 179). Nonetheless, the species was treated in more detail in later studies, when an illustration and data from four additional specimens became available (Wied 1824: Vol. 8; Wied 1825: 284). In the original description, ventral and subcaudal scale counts, measurements, general body coloration and the presence of two keeled scale rows were reported as diagnostic characters. The latter character led some authors (e.g., Schlegel 1837: 177; Duméril 1853: 452) to include this species in the synonymy of *Herpetodryas carinatus*. Bailey (1955: 8) later resurrected the taxon, despite suspicions of the weak diagnostic power of this character, in addition to the possible existence of several species under the name of *Herpetodryas carinatus* (see Cope 1861: 562).

Dixon et al. (1993) evaluated the variability of the traditional morphological characters (e.g., color pattern, measurements and scale counts) for *Chironius bicarinatus* and pointed out some differentiation in color pattern, the sum of ventral and subcaudal scale counts, number of maxillary teeth, and a higher incidence of temporal scales formula 1+1 in the southernmost populations. Neverthe-

less, the authors did not propose taxonomic acts related to these variations due to the limited number of samples and evidence of the overlapping of some characters. These authors only indicated the possibility of the existence of two subspecies under the name *C. bicarinatus* distributed throughout the Atlantic Forest, one in gallery and coastal forests and the other in ombrophilous dense and semideciduous forests. Entiauspe-Neto et al. (2020) reviewed *C. bicarinatus* based on morphological and molecular data and described the aforementioned southernmost populations of *C. bicarinatus* as a distinct taxon, *C. gouveai*.

Currently, the proposed diagnoses for *Chironius bicarinatus* reflect a wide variability in color pattern and pholidosis (Dixon et al. 1993; Entiauspe-Neto et al. 2020). Given the long and convoluted taxonomic history of *C. bicarinatus* and its massive morphological variability, herein, we investigate the variability of phenotypic characters throughout the entire distribution of *C. bicarinatus* based on geographically representative samples, reporting data on meristic and morphometric characters, color pattern, hemipenial morphology, and cranial osteology in agreement with other lines of evidence (i.e., molecular phylogeny and environmental niche modeling), in order to accurately infer species boundaries (see de Queiroz 2007; Pante et al. 2015). We conclude that *C. bicarinatus* actually refers to a species complex that requires taxonomic changes to accurately reflect the lineage diversity. Due to taxonomic inconsistencies in *C. gouveai* found in the course of the present study, we refine and rectify data on its distribution through environmental niche modeling and assess the variability of morphological and molecular characters of this species to infer the boundaries between it and *C. bicarinatus*. In addition, we diagnose a distinct lineage without an available name and thus describe this new species whose distribution is restricted to the Baturité Massif, a relictual and isolated rainforest in the Caatinga xerophytic domain, in the state of Ceará, northeastern Brazil.

Materials and Methods

Examined Specimens and Taxonomic Comparisons

We examined 485 specimens from 227 localities currently attributable to the *Chironius bicarinatus* complex (*C. bicarinatus*, *C. gouveai*, and Baturité Massif sample) housed in 35 scientific collections covering the species' distribution to assess the variability in morphological characters (see Appendix 1). The comparisons supporting our taxonomic decisions are based mainly on the examined specimens, but also on the original descriptions of all valid congeners, including information on the holotype of *C. gouveai* (Entiauspe-Neto et al. 2020), and the diagnoses proposed by Dixon et al. (1993). Regarding the *Chironius* taxa sympatric to the *C. bicarinatus* species complex [i.e., *C. carinatus* (Linnaeus, 1758), *C. exoletus* (Linnaeus,

us, 1758), *C. foveatus* Bailey, 1955, *C. fuscus* (Linnaeus, 1758) and *C. laevicollis* (Wied, 1824)], only *C. exoletus* deserves special attention for presenting a coloration pattern and meristic characters which partially overlap those of the *C. bicarinatus* complex. Thus, we also examined a representative sample of Atlantic Forest specimens of *C. exoletus* ($n = 464$) in order to clarify the identities of both species (hereafter represented as *Chironius* cf. *exoletus* since it also represents a species complex under ongoing study by the senior author; see Sudré et al. 2014; Hamdan et al. 2017; Torres-Carvajal et al. 2019a).

Geographical Data

We retrieved the geographic coordinates (datum WGS84) based on institutional catalogs or databases (Appendix 1) and, whenever possible, they were refined with the aid of Gazetteers (e.g., Paynter and Traylor 1991) or additional software (e.g., Google Earth). The map and spatial analyses were performed using the software QGIS v.3.30 (QGIS Development Team 2023) and the statistical software R (R Core Team 2022) with specific packages indicated below, respectively.

Meristic and Morphometric Characters

The meristic characters mostly follow those used by Dixon et al. (1993), as did the methods for counting scales and teeth, and the standardized notations for reporting data. The main qualitative characters analyzed were: keel intensity in the dorsal rows (weak or strong), body coloration, presence of a postocular stripe, band pattern along the body, presence of apical pits along the body and condition of the cloacal plate (divided or entire). Some specimens had a small scale in the anterior temporal, which we refer to as an accessory scale. The color pattern characteristics mostly reflect those of preserved specimens, but we also provide data obtained from the photographic material of specimens while alive [databases of Museo Argentino de Ciencias Naturales (MACN); Museo Nacional, Universidade Federal do Rio de Janeiro (MNRJ); and iNaturalist]. Appendix 2 contains the iNaturalist observation codes used in this study. We performed frequency analyses among operational taxonomic units with respect to the qualitative characters that exhibit some degree of polymorphism that might be informative (see below in the “Determination of Operational Taxonomic Units” section, on how the operational taxonomic units were delimited). Additionally, special attention was given to other potentially informative qualitative characters with respect to the shape and contact of head scales and body scales ornamentation.

The morphometric characters used in this study were: head height (at highest point), head width (at widest point), head length (from snout tip to quadrate mandibular articulation), orbit diameter (on right side only), nostril-orbit distance, snout length (from snout tip to anterior border of right orbit), distance between nostrils, and snout

width (at loreals level). All of the aforementioned characters were measured with a dial caliper to the nearest 0.01 mm, except for snout–vent length (SVL) and caudal length (CL) measured using a tapeline to the nearest 1.0 mm. Sex was determined based on the presence/absence of hemipenes. When the organs were not evident, we performed a small incision on the midventral surface of the tail (Pesantes 1994).

Anatomical Preparations

Hemipenes preparations followed a combination of techniques proposed by Pesantes (1994) and the changes detailed by Passos et al. (2016), regarding the replacement of KOH with distilled water, and the process of staining calcareous structures with an alcoholic solution of Alizarin Red originally proposed by Uzzell (1973) as modified by Nunes et al. (2012). Terminology regarding hemipenial morphology follows the terms and definitions used by Dowling and Savage (1960) and Zaher (1999). We did not prepare the hemipenes of some fixed specimens with fully everted and not fully expanded hemipenes (FUNED 2893, IBSP 55660, MACN 47893, MCP 3724, MCP 3730, MCP 3839, MCP 4305, MNHN 1794, MNRJ 4693, MNRJ 10829, MNRJ 22017, MNRJ 23371, MNRJ 12921, MNRJ 14983, MNRJ 15614, MNRJ 16110, MNRJ 21049, MZUSP 11578, ZUEC 925, ZUEC 1011, ZUEC 1347, ZUEC 1420, ZUEC 3968, MHNBA 1858), but they were analyzed during the same period of specimen examination or later, through the use of photographs. Regarding skull analyses, dry prepared specimens (MCP 4305, MCP 19414, MNRJ 14488, MNRJ 18926) were examined and some specimens (MNRJ 27717, MNRJ 20049, ZUFMS 1686) were selected for scanning using a Skyscan 1173 in-vivo high-resolution μ CT scan at the Nuclear Instrumentation laboratory COPPE/UFRJ, Instituto Alberto Cruz Coimbra de Pós-Graduação e Pesquisa de Engenharia, Universidade Federal do Rio de Janeiro (UFRJ), state of Rio de Janeiro, Brazil. The scanned specimens were visualized in CTvox 2.6 (Bruker MicroCT) for the examination of osteological characters and the final images were edited in Adobe Photoshop CS6 2 (Adobe Inc., 2019). The nomenclature for cranial osteology follows the terms and definitions used by Cundall and Irish (2008), Klaczko et al. (2014), Hamdan and Fernandes (2015), Torres-Carvajal et al. (2019b), and Entiuspe-Neto et al. (2020).

Species Concept and Species Delimitation

Herein, the term “species” refers to separately evolving metapopulation lineages (sensu de Queiroz 2007). As species delimitation criteria, we considered the correspondence between the clades recovered in the DNA-based phylogenetic trees and the presence of one or more apparently fixed exclusive diagnostic morphological characters. We used a tolerance of 95% intervals to allow levels

of polymorphism (e.g., sensu Wiens and Servedio 2000) that showed statistical confidence in our sample and to allow for a putative taxon to be distinguished from the others in the *Chironius bicarinatus* complex. Therefore, if an OTU (see “Determination of Operational Taxonomic Units” section) shows correspondence in the aforementioned parameters, we consider that OTU a valid species. In addition to the operational criteria, using morphological and molecular approaches (e.g., geographic variation, multivariate analyses, molecular phylogeny) to infer species’ boundaries, we also integrated ecological evidence (e.g., environmental niche modeling) to test whether species occupy distinct environmental niches and thereby, increase the power of species delimitation (de Queiroz 2007; Padial et al. 2010).

Determination of Operational Taxonomic Units

The delimitation of operational taxonomic units (a definition used prior to data analysis for ordering groups that share a given set of observed characters; Sneath and Sokal 1973) in this study was guided by the results of the phylogenetic analysis and the variations in qualitative and quantitative (discrete and/or continuous) characters reflecting (or not) the search for morphological discontinuity throughout the species’ distribution (see Dixon et al. 1993). When sampling the *Chironius bicarinatus* complex, we found that some quantitative (e.g., number of ventrals, subcaudals, temporals, supralabials in contact with the orbit, and maxillary teeth) and qualitative characters (e.g., presence and number of keeled dorsal rows, presence of apical pits along the body, and general body coloration) were potentially informative, due to variations that may be related to geographical distribution. Thus, a brief biogeographical description of each operational taxonomic group is presented as follow:

Chironius bicarinatus.—Comprised specimens from coastal forests from the south of the São Francisco River (in the state of Sergipe, northeastern region of Brazil) to the Serra do Tabuleiro (in the state of Santa Catarina, southern region of Brazil).

Chironius gouveai.—Contained specimens from inland Serra do Mar at higher elevations in Pampas, Mixed and Semideciduous Forests, below the Paranapanema River and bounded to the west by the Paraná River.

Baturité Massif sample.—Included specimens restricted to the “Brejo de Altitude” of the Baturité Massif (state of Ceará, northeastern Brazil), above the São Francisco River.

Statistical Analyses

Statistical tests were performed based on meristic and morphometric characters to assess sexual dimorphism

(ANOVA test) and other possible differences between operational taxonomic groups (Tukey HSD test). We used Shapiro-Wilk and Levene tests to assess assumptions of normality and homoscedasticity, respectively, for the original variables. Confirming these assumptions ($p > 0.05$), sexual dimorphism was evaluated using an ANOVA test, applied individually to each operational taxonomic group. In the case of sexual dimorphism, males and females were treated separately in subsequent statistical tests. Then, we applied the Tukey HSD test to report differences between the groups, comparing distinct groups and we posteriorly evaluated which pairs of groups showed differences. When the tests refuted assumptions of normality and/or homoscedasticity, we employed nonparametric procedures to compare means (Mann-Whitney U, Kruskal-Wallis, Games-Howell) (Zar 2010; McDonald 2014). The variables that were investigated regarding sexual dimorphism and differences between groups were: caudal length/total length (CL/TL) ratio, counts of ventral scales (VEN), subcaudal scales (SUB), and maxillary teeth (MT).

In order to avoid analytical noise due to ontogenetic allometry, the analyses involving morphometric characters only included supposedly mature specimens. We established the maturity cut-off based on an ongoing reproductive study of the *Chironius bicarinatus* complex (G.S. Araújo and S. Almeida-Santos, pers. comm. on August 16, 2022), where the size of the smallest mature individual was 580 mm SVL for males and 630 mm SVL for females considering both, *C. bicarinatus* and *C. gouveai*. As the specimens restricted to Baturité Massif are significantly smaller in body size, regarding the first two species, and since we aimed to reach a reasonable maturity cut-off for this sample, we opted to follow the results presented in Pinto et al. (2010), which addressed the reproductive biology of *Chironius flavolineatus* (Jan, 1863) and *C. quadricarinatus* (Boie, 1827). Although these taxa are relatively smaller than *C. bicarinatus* and *C. gouveai*, the body size of their populations appears to be equivalent to the Baturité Massif sample. Therefore, we established 450 mm SVL as the maturity cut-off for both, males and females from the samples restricted to the Baturité Massif.

Based on the results of the variance analyses, we performed a Discriminant Function Analysis (DFA) using a subset of specimens containing no missing data for the following 11 log-transformed exploratory variables: ventral (VEN), maxillary teeth (MT), snout-vent length (SVL), head height (HH), head width (HW), head length (WL), orbit diameter (OD), nostril-orbit distance (NOD), snout length (SL), distance between nostrils (DN), and snout width (SW). Missing values were only replaced with group mean for maxillary teeth (MT). These variables were selected according to their distribution identified during data collection, using those whose variation proved to be potentially informative for comparisons between the groups. Although subcaudal (SUB) and caudal length (CL) proved to be potentially informative variables for discrimination, they were not incorporated into the multivariate analyses because of the limited num-

ber of specimens that still had their entire tail due to the high proportion of excised tails (see Moura et al. 2022). The assumptions of covariance matrix homogeneity and the absence of multicollinearity between the exploratory variables, were verified before the analyses (Manly 2000). We also performed the leave-one-out cross-validation procedure to assess the accuracy of the DFA's group reclassification. Subscripts of our statistics reflect degrees of freedom. All statistical tests were performed using STATISTICA 10.0 (StatSoft 2011) and PAST 4.13 (Hammer et al. 2001) software. Our descriptive data reflect "minimum–maximum ([95% confidence intervals] \pm SD, n = sample size)".

Molecular Data and Phylogenetic Analysis

Aiming to assess the phylogenetic relationships within the *Chironius bicarinatus* complex and the phylogenetic position of Baturité Massif sample within the genus, we included all representatives of the genus *Chironius* currently available on GenBank and representatives of the eight other Colubridae genera (*Dendrophidion* Fitzinger, 1843, *Drymarchon* Fitzinger, 1843, *Drymobius* Fitzinger, 1843, *Drymoluber* Amaral, 1930, *Leptophis* Bell, 1825, *Mastigodryas* Amaral, 1934, *Oxybelis* Wagler, 1830, and *Spilotes* Wagler, 1830). The tree was rooted with *Dipsas catesbyi* (Sentzen, 1796). We selected specific outgroup terminals in order to maximize character coverage (i.e., homologous sequences available from GenBank) and phylogenetic structure according to the trees of the four most densely sampled *Chironius* phylogenies (Klaczko et al. 2014, Hamdan et al. 2017, Torres-Carvajal et al. 2019a, Entiauspe-Neto et al. 2020). We compiled the complete or partial sequences of four molecular markers: mitochondrial genes for 12S rRNA (12S), 16S rRNA (16S), and subunit IV of NADH dehydrogenase (ND4); and nuclear oocyte maturation factor (c-mos). Specimen information and GenBank accession numbers used in this study are provided in Appendix 3. We checked all available vouchers of the *Chironius bicarinatus* complex, from which the sequences were extracted by first-hand examination, except for LCBB 18, 21, MAP-T 956 (no preserved voucher for examination), CHFURG 4394 and ZFMK 103132. We tentatively identified MAP-T 956 as *C. gouveai* based on its geographic origin, since there is no record of *C. bicarinatus* in our sample from this region (see Appendix 1). In addition, the latter two specimens (CHFURG 4394 and ZFMK 103132) were illustrated by Entiauspe-Neto et al. (2020), allowing us to confirm its identification.

We generated new DNA sequences for species of the *Chironius bicarinatus* complex, including three mitochondrial gene segments (12S rRNA, 16S rRNA, ND4) and one nuclear gene segment (c-mos). In total, 12S rRNA, 16S rRNA and c-mos sequences were generated for nine specimens of *C. bicarinatus*, three of *C. gouveai*, and four of Baturité Massif sample, while ND4 sequences were generated for two *C. bicarinatus* specimens and two

specimens from the Baturité Massif sample. Localities and voucher information are provided in Appendix 3. We performed PCRs using a PCR Master Mix and a pair of primers for each segment (Appendix 4). Thermocycling for DNA amplification for the first partition is provided in Appendix 4. The size and quality of the resulting PCR products were confirmed by electrophoresis through a 1% agarose gel, stained and visualized under a UV Image capture and analysis system. PCR products were purified and sent to the Centro de Estudos do Genoma Humano e Células-Tronco from Universidade de São Paulo and Rede de Plataformas Tecnológicas da Fundação Oswaldo Cruz, both in Brazil. The resulting electropherograms for both DNA strands were analyzed using CHROMAS LITE 2.01 (Technelysium Pty Ltd), edited using MEGA X (Kumar et al. 2018) and adjusted manually to generate consensus sequences for each specimen. Sequences were checked using the basic local alignment search tool (Altschul et al. 1997) against the GenBank nucleotide database to ensure that the amplified product was correct and not contaminated. In total, 252 sequences of 81 *Chironius* specimens were sampled, including 72 sequences of 23 specimens of the *C. bicarinatus* complex (23 for 12S, 23 for 16S, 22 for c-mos, and 4 for ND4) and 180 sequences of 58 specimens of 18 other *Chironius* taxa (51 for 12S, 49 for 16S, 54 for c-mos and 26 for ND4). All the aforementioned sequences were aligned using MAFFT 7 (Katoh et al. 2002), with a gap opening penalty of 1.53 and an offset value of 0.0 (Thompson et al. 1994). Parameters for c-mos, and ND4 were left at their default settings (L-INS-i model) and parameters for 12S and 16S were set to the E-INS-i model. We aligned each segment separately, and segments were concatenated using MESQUITE 3.10 (Maddison and Maddison 2016), to a total of 2,284 bp. We partitioned the data set by locus and selected the appropriate models of the DNA sequences using the software jModeltest 2.17 (Posada 2008) based on the Akaike information criterion or AIC (Akaike 1974). The models obtained were HKY + G for c-mos, and GTR + G + I for ND4, 12S, and 16S.

We performed a partitioned Bayesian Inference (BI) using MrBayes 3.2.2 (Ronquist and Huelsenbeck 2003) through the portal CIPRES Science Gateway (Miller et al. 2010) with the concatenated dataset and the partition models described. Each analysis included four independent runs of 5,000,000 generations with four chains of Markov Chain Monte Carlo. Parameters and trees were sampled every 5,000 generations and using a random tree as a starting point. We considered the convergence of the runs when the standard deviation of the frequency splits was lower than 0.05 and by observing ESS values above 300 in Tracer 1.4 (Rambaut and Drummond 2007). The first 25% of the samples were discarded as burn-in. Branch support was assessed by posterior probability, and nodes with posterior probabilities > 0.95 were considered strongly supported (Matioli and Fernandes 2012). Additionally, we used the mitochondrial 16S rRNA fragment to calculate the genetic distances (maximum intraspecific and minimum interspecific) between the species of *Chironius*. This marker has the characteristics for use as a

standard DNA barcoding marker for vertebrates to complement COI (see Vences et al. 2005). We estimated the uncorrected pairwise distances using MEGA X (Kumar et al. 2018), with pairwise deletion of missing information.

Niche Modeling and Niche Overlap

Environmental variables and occurrence data treatment

We generated model projections for *Chironius bicarinatus* and *C. gouveai* to predict species distribution over time, in addition to testing the degree of niche overlap in the environmental space for each pair of species of the *C. bicarinatus* complex. We downloaded 19 bioclimatic variables for the current climate from the CHELSA database (Karger et al. 2017) and aggregated the data to a resolution of 5 arcmin using the raster package (Hijmans 2023). We also used elevation data (SRTM) (Farr and Kobrick 2000), which we transformed into relief roughness (raster package; Hijmans 2023), that is the maximum difference in elevation between the focal cell and its neighbors. To reduce issues with multicollinearity, we used Variance Inflation Factor (VIF) (usdm R package; Naimi et al. 2014), only selecting variables with $VIF < 10$. Although we recognize that this selection could remove a variable that is more direct for a species' niche than a highly collinear one that was selected, we discuss the importance of variables, taking into consideration groups of similar variables. From this initial selection, we kept the following non-collinear variables: Bio 10, Bio 13, Bio 14, Bio 18, Bio 19, Bio 2, Bio 3, Bio 8 and relief roughness. To project the models into past climates, we also obtained the same set of variables estimated for Middle Holocene (6 kyr), the Last Glacial Maximum (21 kyr, LGM), and the Last Interglacial (120 kyr, LIG) from the PaleoClim database (Brown et al. 2018). All variables were cropped to a 5-degree buffer around the species-points, which defined the background and projecting area for the models. To decrease spatial autocorrelation due to the clustering of occurrence records in areas with denser sampling effort, we performed spatial thinning, keeping unique occurrence records at a distance of at least 15 km apart with the spThin v.3.6 R package (Aiello-Lammens et al. 2015).

Modeling procedure

We used the ENMeval R package (Muscarella et al. 2014) for the modeling procedure below. First, we performed a model selection for the MaxEnt algorithm (Hijmans et al. 2017; Phillips et al. 2006) with several distinct parameters. We used regularization multipliers ranging from 0.5 to 5 (increments of 0.5) and three feature class combinations (“L”, “LQ”, “LQP”; where L = linear, Q = quadratic, P = product), but avoiding more complex ones (e.g., hinge, threshold) as we were projecting models to a different time. Analyses were performed with the ENMeval function with 1,000 points of pseudo-absence (background) and partitioning the data in test and training with

“checkerboard2” for the cross-validation bins. This data partition scheme further reduces the effects of spatial sampling bias and spatial autocorrelation (Muscarella et al. 2014). Variable importance and their contributions to the model's performance were obtained through the jackknife tests with the ENMeval function (Phillips et al. 2006). Model performance was evaluated with the area under the curve (AUC) and the true skill statistics (TSS). We then selected the models with delta-AICc lower than 10, averaging the selected models by AUC (if more than one) for model projection (both current and past conditions).

Niche overlap

We used the ecospat R package and the functions niche.overlap, niche.equivalency.test, niche.similarity.test for measuring and testing niche overlap between species (Broennimann et al. 2023). We measured the niche overlap observed for each species-pair with Schoener D metric (Schoener 1968), which ranges from 0 (no overlap/complete divergence) to 1 (complete/high overlay) and we tested the significance of the metric against two different null distributions (niche equivalence and niche similarity; Warren et al. 2008). The equivalence tests evaluate if there is significant overlap in niches as determined by the environmental conditions in the species' records, whereas similarity tests assess if the niches of one species significantly overlaps with the conditions found across the entire range of the other species (i.e., not only across the species records). Niche equivalence is rejected if observed niche overlap falls within the 95% of the null distribution. Niche similarity is rejected if niche overlap is lower than 95% of null the distribution values. We used the PCAenv approach to estimate the environmental space occupied by each species across the same set of variables used in the niche modeling following Broennimann et al. (2012) and Di Cola et al. (2017). For the Baturité Massif sample, we used a small buffer of 0.1 degrees around the records to gather enough environmental information for the analyses.

Results

Phylogenetic Analysis and Genetic Distances

For the *Chironius bicarinatus* complex, 48 new sequences for 16 specimens were generated, with 15 sequences for each 12S and 16S fragment, 14 for c-mos and 4 for ND4 (see Appendix 3). The total aligned length of the dataset was 2,166 base pairs (bp). We retrieved a tree topology based on BI recovering at least twelve species within *Chironius* (*C. bicarinatus* complex, *C. brazili*, *C. flavolineatus*, *C. multiventris*, *C. exoletus*, *C. flavopictus*, *C. monticola*, *C. laevicollis*, *C. scurrulus*, *C. fuscus*, *C. grandisquamis* and *C. challenger*) as monophyletic (pp = 1). Additionally, we recovered Baturité Massif sam-

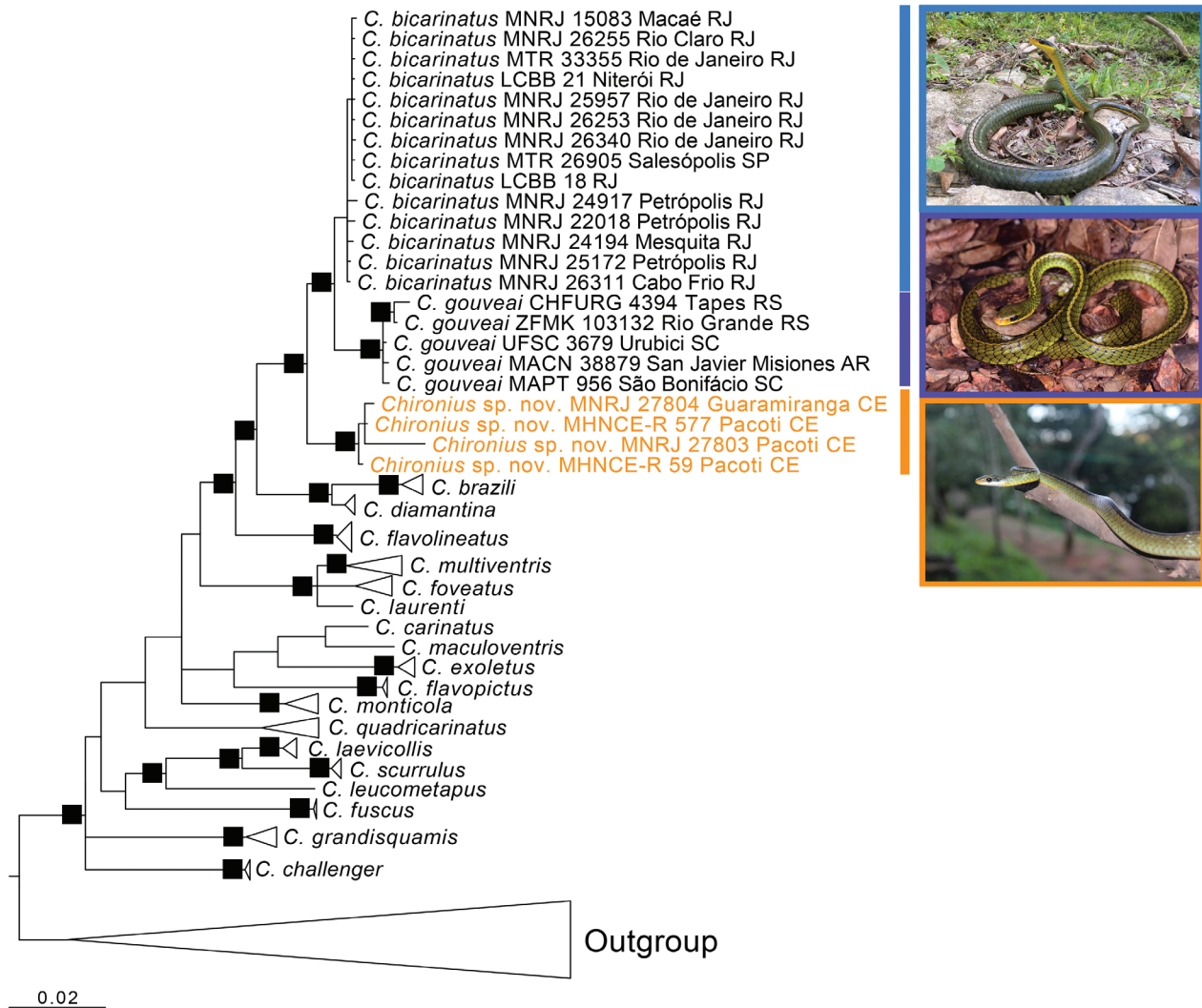


Figure 1. Phylogenetic relationships of the *Chironius bicarinatus* complex estimated under Bayesian Inference based on four molecular markers (12S, 16S, ND4, c-mos) concatenated from a final matrix of 2,166 bp. Only posterior probabilities above 0.95 are shown for the sake of clarity as black squares at nodes. *Chironius bicarinatus*: blue; *C. gouveai*: purple; *Chironius* sp. nov. (= Baturité Massif sample): orange. The detailed phylogenetic tree is provided as Supplementary Material (Fig. S1). Photos by S. Marques-Souza (*C. bicarinatus*), M. Borges-Martins (*C. gouveai*), and J.A. Oliveira (*Chironius* sp. nov.).

ple, nested within the *Chironius bicarinatus* clade, strongly supported ($pp = 1$) as the sister-group of the clade *C. bicarinatus* + *C. gouveai* (Fig. 1), which was congruent with the grouping based on morphological characters (see below). All aforementioned relationships are supported by high posterior probabilities ($pp > 0.95$). However, since checking the identification of most of the sequences of the other *Chironius* spp. available on GenBank is beyond the aim of the present study, except those of the *C. bicarinatus* complex, we refrain from commenting on the interrelationships retrieved (see Fig. S1 for the detailed phylogenetic tree). Regarding the genetic differences calculated from the uncorrected pairwise genetic distances for sequences of 16S rRNA, *Chironius* species differed from other colubrid genera from 5.7–14.0%. Within the *C. bicarinatus* complex, genetic distances range from 0.4–4.0%, and the complex distance from its congeners from 2.0–10.0%. *Chironius bicarinatus* is 0.4–3.7% divergent from *C. gouveai*, while the Baturité Massif sample is 1.9–4.0% divergent from *C. gouveai* and 1.5–2.8%

from *C. bicarinatus*. Within the four sequences of Baturité Massif sample, distance ranges from 0.2–0.7%. See Table S1 for the detailed genetic differences among species of *Chironius* for sequences of 16S rRNA.

Quantitative Analyses

Table 1 shows the variability in meristic and morphometric characters for each defined group in the *Chironius bicarinatus* complex. A detailed report of the morphological data of specimens examined is provided as Supplementary Material (Table S2). We detected sexual dimorphism in all the characters analyzed for at least one of the three operational taxonomic groups. Ventral counts were higher in females of *C. bicarinatus* ($U = 5083.000$; median = 158 and 157, for females and males, respectively, hereafter; $p < 0.01$), *C. gouveai* ($F_{1,138} = 76.54$; $p < 0.0001$), and Baturité Massif sample ($U = 130.000$; median = 156 and 154; $p = 0.0001$); subcaudal counts and CL/TL ra-

Table 1. Comparisons of quantitative characters between the three determined groups of the *Chironius bicarinatus* complex. Descriptive data reflect “minimum–maximum ([95% confidence intervals] ± SD, n = sample size)”. Abbreviations: ventrals (VEN), subcaudals (SUB), maxillary teeth (MT), snout-vent length (SVL), caudal length (CL), head height (HH), head width (HW), head length (HL), orbit diameter (OD), nostril-orbit distance (NOD), snout length (SL), distance between nostrils (DN), and snout width (SW).

	Females			Males		
	<i>C. bicarinatus</i>	<i>C. gouveai</i>	Baturité Massif sample	<i>C. bicarinatus</i>	<i>C. gouveai</i>	Baturité Massif sample
VEN	147–170 (158.0 [157.0, 159.0] ± 5.0, 103)	156–174 (163.8 [162.8, 164.8] ± 3.7, 60)	154–162 (156.7 [155.9, 157.4] ± 2.2, 34)	145–165 (155.8 [155.1, 156.6] ± 4.5, 130)	151–167 (158.6 [157.9, 159.3] ± 3.3, 80)	149–159 (153.6 [152.9, 154.7] ± 2.1, 27)
SUB	130–157 (140.4 [137.8, 142.9] ± 6.8, 30)	139–146 (141.8 [140.2, 143.4] ± 2.2, 10)	124–135 (129.3 [127.7, 130.9] ± 2.7, 14)	125–154 (140.3 [138.1, 142.6] ± 7.6, 45)	131–152 (141.2 [139.1, 143.4] ± 5.0, 23)	132–138 (133.6 [131.3, 136.0] ± 2.2, 6)
MT	31–38 (34.3 [33.8, 34.8] ± 1.7, 45)	28–36 (31.8 [31.0, 32.6] ± 1.9, 25)	35–39 (36.0 [35.4, 36.6] ± 1.3, 21)	30–37 (33.9 [33.6, 34.3] ± 1.5, 63)	27–34 (30.4 [29.9, 30.9] ± 1.5, 39)	34–36 (35.1 [34.8, 35.4] ± 0.5, 16)
SVL	632.0–1170.0 (789.4 [758.6, 820.2] ± 112.8, 54)	662.0–955.0 (797.6 [775.5, 819.7] ± 66.3, 37)	460.0–658.0 (566.0 [548.5, 584.2] ± 47.7, 29)	585.0–1162.0 (849.9 [821.9, 878.0] ± 135.5, 92)	606.0–1010.0 (774.9 [747.2, 802.6] ± 102.5, 55)	470.0–739.0 (593.7 [552.8, 634.5] ± 84.7, 19)
CL	350.0–610.0 (440.1 [405.0, 475.1] ± 65.7, 16)	430.0–525.0 (472.5 [439.8, 505.2] ± 31.2, 6)	272.0–347.0 (301.9 [287.3, 316.5] ± 24.1, 13)	350.0–640.0 (459.9 [430.4, 489.5] ± 81.9, 32)	388.0–535.0 (465.3 [443.3, 487.3] ± 41.2, 16)	260.0–352.0 (310.6 [275.9, 345.4] ± 33.1, 6)
HH	7.6–13.5 (10.2 [9.5, 10.9] ± 1.5, 23)	8.0–12.7 (10.2 [9.6, 10.8] ± 1.3, 21)	6.3–8.4 (7.4 [7.0, 7.8] ± 0.5, 11)	8.1–14.2 (10.9 [10.4, 11.4] ± 1.7, 44)	7.1–13.1 (10.2 [9.6, 10.8] ± 1.5, 26)	6.3–9.1 (7.9 [7.1, 8.8] ± 0.9, 7)
HW	9.3–16.9 (12.7 [12.1, 13.5] ± 1.6, 23)	10.8–15.1 (13.0 [12.5, 13.5] ± 1.2, 21)	8.0–10.3 (9.3 [8.7, 9.8] ± 0.8, 11)	9.7–18.7 (13.7 [13.0, 14.4] ± 2.3, 44)	9.4–16.2 (12.9 [12.1, 13.6] ± 1.8, 26)	8.6–10.9 (10.0 [9.3, 10.6] ± 0.7, 7)
HL	19.8–30.3 (23.4 [22.3, 24.6] ± 2.6, 23)	19.0–27.6 (23.6 [22.8, 24.5] ± 1.8, 21)	17.3–20.8 (18.7 [17.9, 19.5] ± 1.2, 11)	19.6–28.8 (24.5 [23.6, 25.4] ± 2.8, 44)	17.7–28.4 (23.4 [22.3, 24.5] ± 2.7, 26)	16.4–20.4 (19.3 [17.9, 20.6] ± 1.4, 7)
OD	5.4–8.3 (6.4 [6.1, 6.7] ± 0.7, 23)	5.7–7.8 (6.6 [6.4, 6.8] ± 0.5, 21)	4.6–6.0 (5.2 [4.9, 5.4] ± 0.3, 11)	5.6–8.2 (6.7 [6.5, 6.9] ± 0.7, 44)	5.4–7.7 (6.5 [6.3, 6.8] ± 0.6, 26)	5.0–6.3 (5.7 [5.3, 6.1] ± 0.4, 7)
NOD	4.1–6.2 (4.9 [4.7, 5.2] ± 0.5, 23)	3.7–6.1 (4.8 [4.5, 5.1] ± 0.6, 21)	3.6–4.5 (4.1 [3.9, 4.3] ± 0.3, 11)	4.1–6.6 (5.3 [5.1, 5.5] ± 0.6, 44)	3.2–6.2 (4.8 [4.5, 5.1] ± 0.7, 26)	3.6–4.5 (4.0 [3.7, 4.4] ± 0.3, 7)
SL	7.1–11.6 (8.9 [8.4, 9.4] ± 1.2, 23)	6.8–11.1 (9.0 [8.6, 9.4] ± 0.9, 21)	6.1–7.8 (6.9 [6.5, 7.2] ± 0.5, 11)	7.2–11.8 (9.5 [9.2, 9.9] ± 1.3, 44)	5.9–11.1 (9.1 [8.6, 9.7] ± 1.3, 26)	6.1–7.7 (7.1 [6.6, 7.6] ± 0.5, 7)
DN	4.5–6.6 (5.3 [5.1, 5.5] ± 0.5, 23)	3.8–6.7 (5.4 [5.1, 5.8] ± 0.8, 21)	3.6–4.8 (4.2 [4.0, 4.4] ± 0.3, 11)	4.2–7.4 (5.7 [5.5, 6.0] ± 0.8, 44)	4.1–7.0 (5.6 [5.3, 5.9] ± 0.8, 26)	3.5–5.3 (4.5 [4.0, 5.0] ± 0.6, 7)
SW	6.0–10.2 (8.3 [7.9, 8.7] ± 1.0, 23)	6.6–10.1 (8.5 [8.1, 9.0] ± 0.9, 21)	5.3–7.0 (6.1 [5.8, 6.5] ± 0.5, 11)	5.6–11.3 (8.9 [8.5, 9.3] ± 1.4, 44)	6.2–10.7 (8.6 [8.2, 9.1] ± 1.2, 26)	5.5–7.3 (6.7 [5.9, 7.4] ± 0.8, 7)

Table 2. Differences for females and males from the three determined groups of the *Chironius bicarinatus* complex (Group 1: *C. bicarinatus*, Group 2: *C. gouveai*, Group 3: Baturité Massif sample) for ventral (VEN) and subcaudal (SUB) counts, caudal length/total length ratio (CL/TL) and number of maxillary teeth (MT).

Variable	Group		Significance		Variable	Group		Significance	
			Females	Males				Females	Males
VEN	1	2	< 0.0001	< 0.02	SUB	1	2		< 0.01
	1	3	< 0.0001	< 0.0001		1	3	< 0.0001	< 0.0001
	2	3	< 0.0001	< 0.0001		2	3	< 0.0001	< 0.0001
CL/TL	1	2			MT	1	2	Females and Males	
	1	3	< 0.0001	< 0.0001		1	3	< 0.0001	
	2	3	< 0.0001	< 0.0001		2	3	< 0.0001	

tio were only higher in males of Baturité Massif sample (U = 8.000; median = 128.5 and 133; p < 0.01, and U = 18.000; median = 0.35 and 0.36; p < 0.05, respectively).

Table 2 reports differences between the groups for ventral and subcaudal counts, CL/TL ratio and number of maxillary teeth.

Table 3. Values (%) of the correct reclassification rate and cross validation analysis (in parentheses) for females and males from the three determined groups of the *Chironius bicarinatus* complex (Group 1: *C. bicarinatus*, Group 2: *C. gouveai*, Group 3: Baturité Massif sample).

			Predicted Group Membership		
		Group	1	2	3
Females	%	1	82.6 (65.2)	13.0 (21.7)	4.3 (13.0)
		2	33.3 (38.1)	66.7 (61.9)	0.0 (0.0)
		3	0.0 (9.1)	0.0 (0.0)	100 (90.9)
Males	%	1	95.5 (93.2)	4.5 (4.5)	0.0 (2.3)
		2	11.5 (11.5)	88.5 (88.5)	0.0 (0.0)
		3	14.3 (14.3)	0.0 (0.0)	85.7 (85.7)

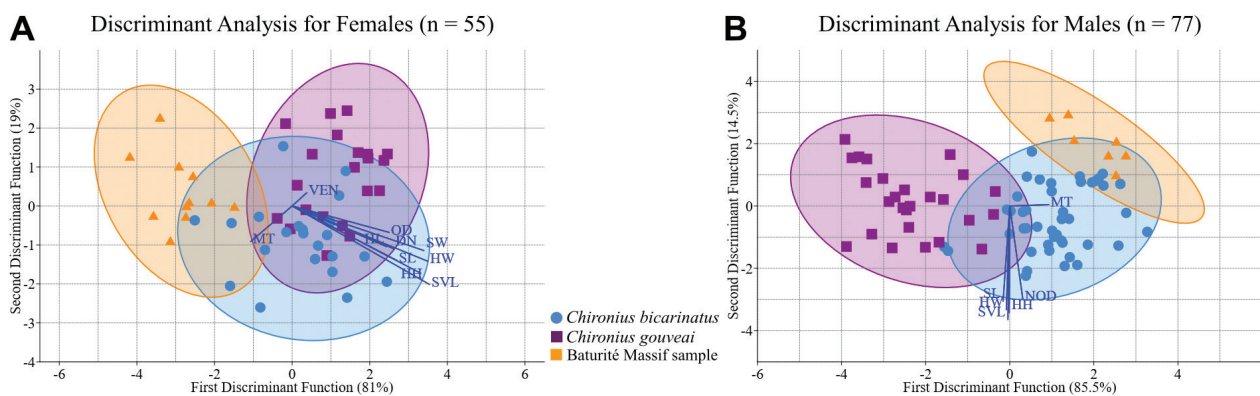


Figure 2. Scatterplots of the scores from two main discriminant functions for the groups of the *Chironius bicarinatus* complex, separating females (A) and males (B). *Chironius bicarinatus*: blue; *C. gouveai*: purple; Baturité Massif sample: orange.

The DFA variables showed statistical significance in group discrimination (Fig. 2). We found that the first function was responsible for most of the differentiation (> 81%) for both males and females. The variables most related to the first function were maxillary teeth (MT; correlation value, hereafter: 0.863) for males, and head width (HW; 0.796), snout width (SW; 0.751), snout-vent length (SVL; 0.723), orbit diameter (OD; 0.709), and head length (WL; 0.662) for females, respectively. In females, the scatterplot shows a large overlap between *Chironius bicarinatus* and *C. gouveai*, and a partial overlap between *C. bicarinatus* and Baturité Massif sample (Fig. 2A). While in males, the discrimination was more evident on both axes, since the variables most related to the second function were: snout-vent length (SVL; -0.903), nostril-orbit distance (NOD; -0.867), head height (HH; -0.825), snout length (SL; -0.823), and head width (HW; -0.792), respectively. The scatterplot shows a partial overlap between the groups, with Baturité Massif sample slightly overlapping with *C. bicarinatus*, when considering the 95% confidence ellipses (Fig. 2B). The results of the discriminant analyses showed accurate reclassification and cross-validated grouped cases in females (80.0%, and 69.1%) and males (92.2%, and 90.9%), respectively (Table 3).

Cumulative Frequency Analyses

We performed cumulative frequency analyses between the groups with respect to the temporal formula, number

of keeled dorsal rows, presence of apical pits along the body and supralabials contacting orbit. For the temporal formula, we observed a higher frequency of temporals 1+1 in *Chironius gouveai* ($n = 93$, 62%), and temporals 1+2 in Baturité Massif sample ($n = 48$, 69%) and *C. bicarinatus* ($n = 167$, 66%). Regarding the number of keeled dorsal rows, in *C. bicarinatus* and *C. gouveai* the keels are usually restricted to two dorsal scale rows ($n = 211$ and 137, 92% and 100%, respectively), while Baturité Massif sample had two ($n = 38$, 67%) or more ($n = 19$, 33%) dorsal keeled rows (2nd–11th dorsal rows). Regarding the presence of apical pits along the body, *C. gouveai* only presents this feature on the neck ($n = 125$, 98%), while Baturité Massif sample has a higher frequency on the neck and in at least one other region of the body ($n = 54$, 98%). On the other hand, *C. bicarinatus* shows closer frequencies, with apical pits only observed on the neck ($n = 99$, 45%) or on the neck, “paravertebrals”, and tail ($n = 116$, 52%). Finally, we observed a higher frequency of three supralabials in contact with the orbit in *C. bicarinatus* ($n = 220$, 96%) and *C. gouveai* ($n = 136$, 96%), while Baturité Massif sample had three ($n = 40$, 62%) or two ($n = 26$, 38%) supralabials contacting the orbit.

Cranial Osteology

For skull analyses, we used four specimens that were previously dry prepared (two of *Chironius bicarinatus* and two of *C. gouveai*) and three scanned specimens repre-

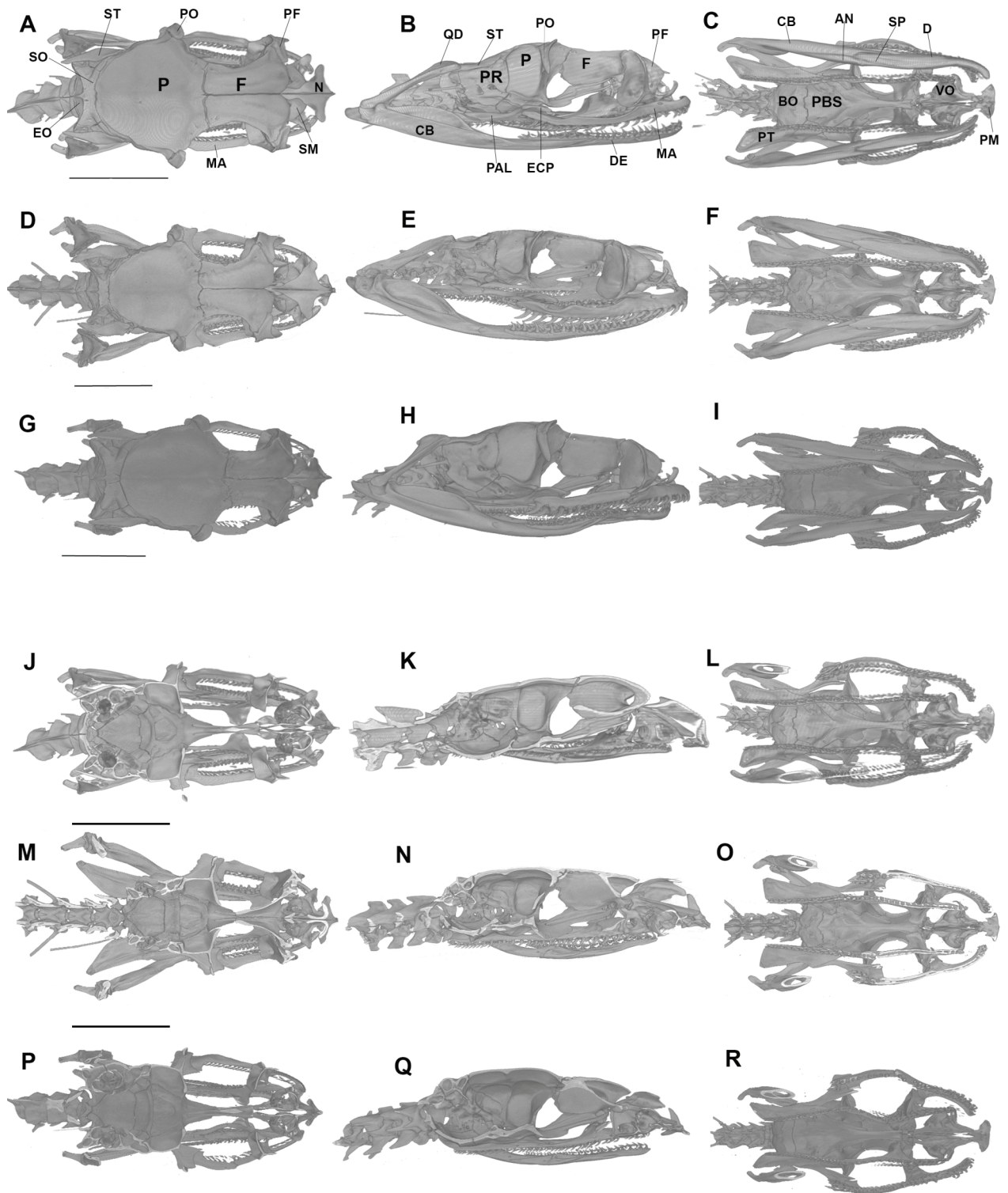


Figure 3. Micro-computed tomography images of the skull for the groups of the *Chironius bicarinatus* complex. Dorsal, lateral, and ventral views of the skulls (A–I) followed by the respective cutaway views (J–R). *Chironius bicarinatus*: A–C, J–L; *C. gouveai*: D–F, M–O; and Baturité Massif sample: G–I, P–R. Scale bar = 5 mm. Abbreviations: AN, angular; BO, basioccipital; CB, compound bone; DE, dentary; ECP, ectopterygoid; EO, exoccipital; F, frontal; MA, maxilla; N, nasal; P, parietal; PAL, palatine; PBS, Parabasisphenoid complex; PF, prefrontal; PM, premaxilla; PO, postorbital; PR, prootic; PT, pterygoid; QD, quadrate; SM, septomaxilla; SO, supraoccipital; SP, splenial; ST, supratemporal; VO, vomer.

senting each of the groups (Fig. 3). Skull comparisons for *C. bicarinatus* (Fig. 3A–C, J–L) were based on dry preparations of the specimens MNRJ 14488 and MNRJ 18926; and a scanned specimen MNRJ 20049 (adult male, SVL 700 mm); for *C. gouveai* (Fig. 3D–F, M–O)

analyses were based on dry preparations of the specimens MCP 4305 (adult male) and MCP 19414; and a scanned specimen ZUFMS 1686 (adult male, SVL 929 mm), as well as the skull information from *Chironius gouveai* paratype (ZFMK 103132, adult male, SVL 720 mm) in

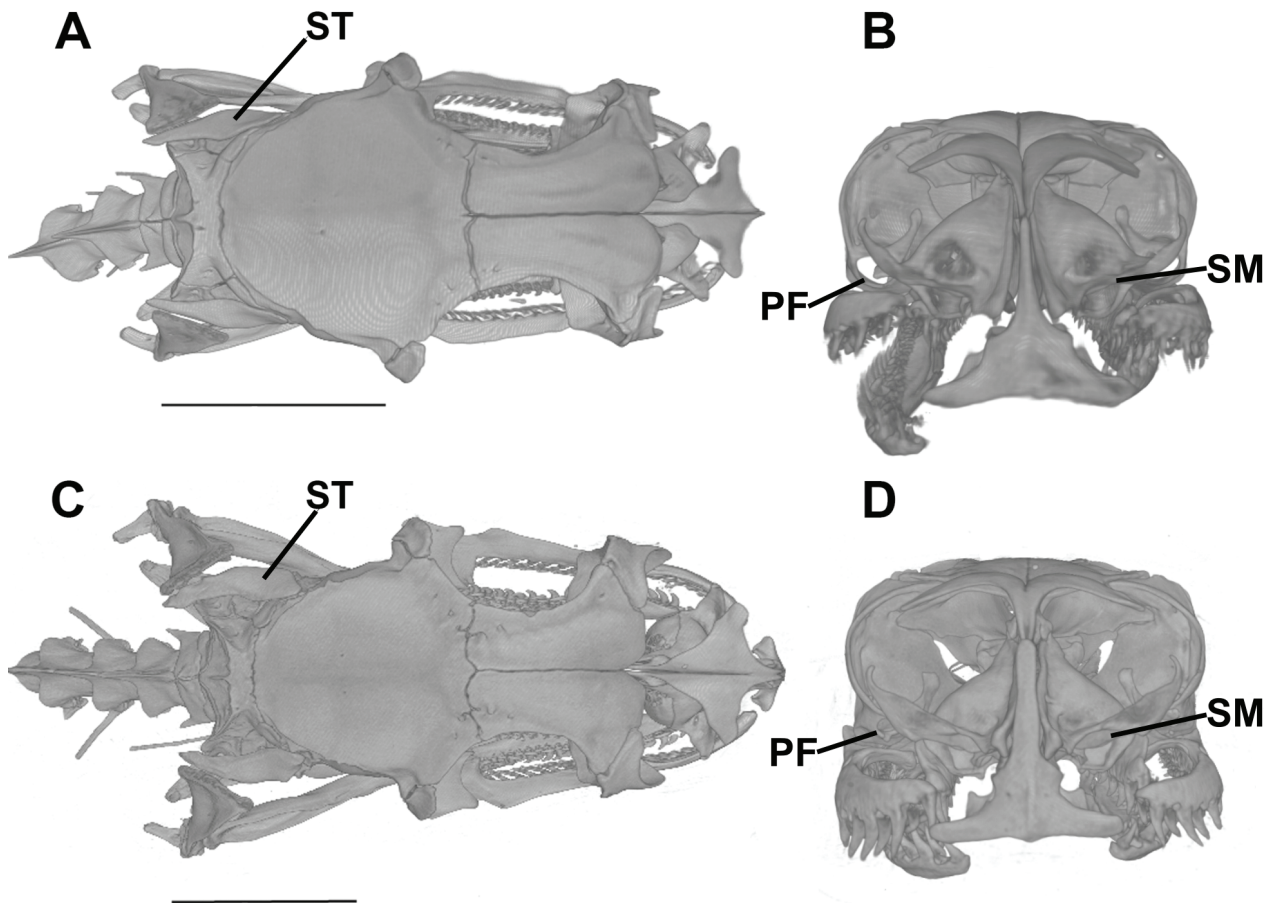


Figure 4. Micro-computed tomography images of the skull showing in detail the diagnostic characters comparing *Chironius bicarinatus* (A, B) and *C. gouveai* (C, D): posterior portion of supratemporal (ST) straight (A) and slightly curved (C); ventral surface of the septomaxilla (SM) smooth (B) and with the presence of a conspicuous projection (D); anteroventral surface of prefrontal lacrimal foramen (PF) smooth (B) and with the presence of a conspicuous projection (D). Scale bar = 5 mm.

the original description (Entiauspe-Neto et al. 2020); and, for Baturité Massif sample (Fig. 3G–I, P–R) the analyses were based on a scanned specimen MNRJ 27717 (adult male, SVL 680 mm).

We found the following differences in the skull comparing *Chironius bicarinatus* with *C. gouveai* (in parentheses): ventral surface of the septomaxilla smooth, $n = 3$ MNRJ 14488, MNRJ 18926, MNRJ 20049 (vs. presence of a conspicuous projection, $n = 2$ ZUFMS 1686, ZFMK 103132); anteroventral surface of prefrontal lacrimal foramen smooth, $n = 1$ MNRJ 20049 (vs. presence of a conspicuous projection, $n = 2$ ZUFMS 1686, ZFMK 103132); posterior portion of supratemporals straight, $n = 3$ MNRJ 14488, 18926, 20049 (vs. slightly curved, $n = 4$ ZUFMS 1686, MCP 4305, MCP 19414, ZFMK 103132); and palatine teeth 23–24, $n = 2$ MNRJ 14488, MNRJ 20049 (vs. 16–18 teeth, $n = 2$ ZFMK 103132, ZUFMS 1686). Figure 4 shows in detail the diagnostic skull characters comparing both groups.

We did not find differences between the skulls of *Chironius bicarinatus* and Baturité Massif sample. On the other hand, we found four differences comparing Baturité Massif sample with *C. gouveai* (in parentheses): ventral surface of the septomaxilla smooth (vs. presence of a conspicuous projection); anteroventral surface of prefrontal lacrimal foramen smooth (vs. presence of a

conspicuous projection); posterior end of supratemporals straight (vs. slightly laterally curved); and palatine teeth 24 (vs. 16–18).

Ecological Niche Modeling

The model selection of the Maxent parameters for *Chironius bicarinatus* provided three models with delta-AICc lower than 10 (Table S3). The averaged model presented an AUC = 0.976 and TSS = 0.85, indicating excellent performance. Areas of high suitability for the current climate closely matched the presence records across lowland Atlantic Forest in the Ombrophilous Dense Forests of southern Bahia and Espírito Santo, Rio de Janeiro and São Paulo States. Model projection to the Last Glacial Maximum showed a potential retraction of suitable areas along the coast of southeastern Brazil and a potential expansion of suitable areas across central regions of Bahia and Pernambuco States. Model projection to the Last Interglacial showed a potential retraction of suitable areas across central regions of Bahia and Pernambuco and a potential expansion of suitable areas along the coast of southern Bahia, Espírito Santo, Rio de Janeiro, São Paulo and Paraná States, as well as small areas of the northeastern Brazilian coast (Fig. 5A). The most important

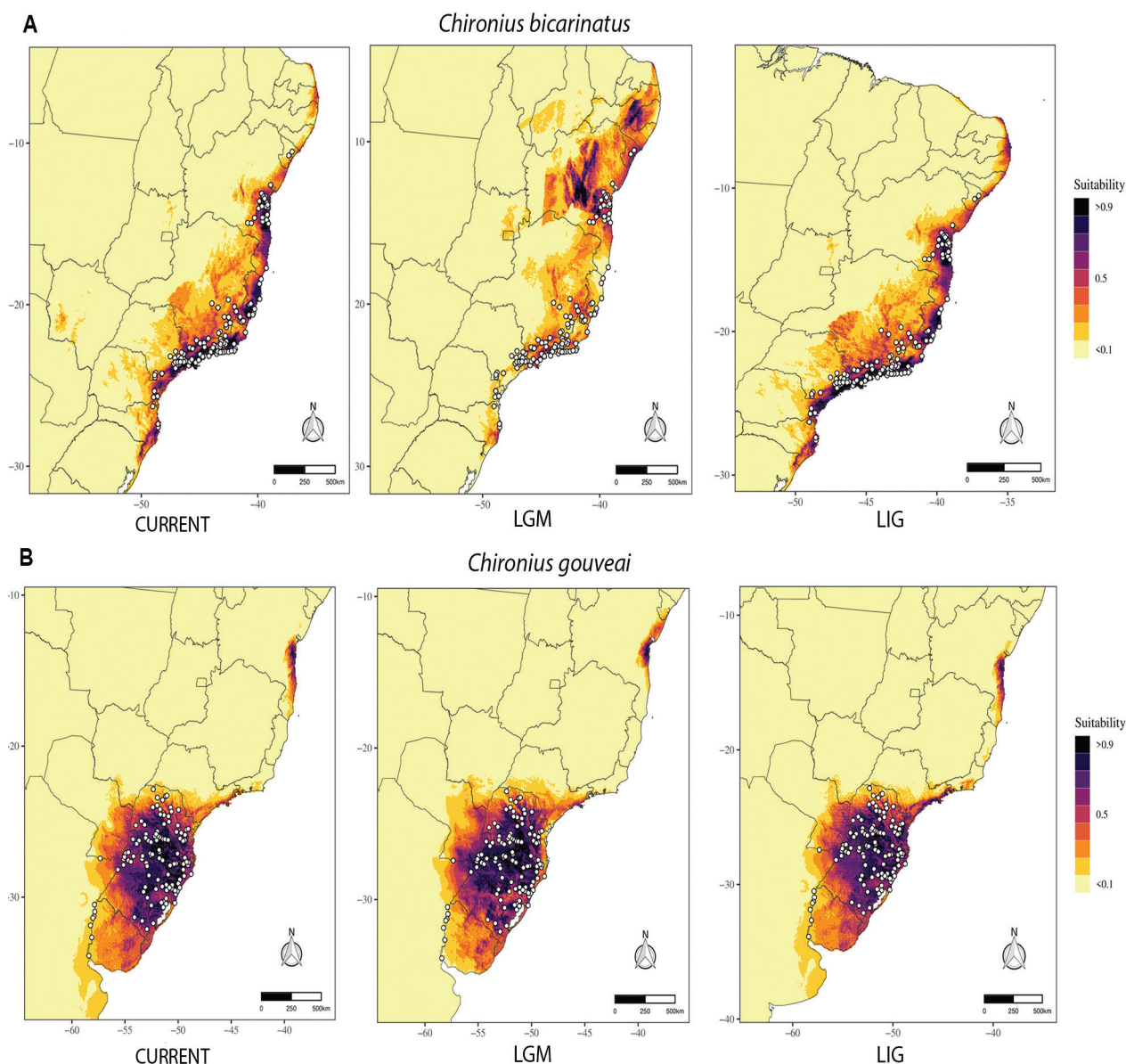


Figure 5. Projection of species distribution modeling for: Current climate, the Last Glacial Maximum (21 kyr, LGM), and the Last Interglacial (120 kyr, LIG) for *Chironius bicarinatus* (A) and *Chironius gouveai* (B).

variable for *C. bicarinatus* was Isothermality (Bio 2), followed by Precipitation of Warmest Quarter (Bio 18 - Table S4).

For *Chironius gouveai*, we obtained four models with delta-AICc lower than 10 (Table S5). The averaged model had AUC = 0.950 and TSS = 0.801, also indicating excellent performance of the modeling procedure. Areas of high suitability in the current climate closely matched the presence records across inland Atlantic Forest in the Mixed Forests of central Paraná and Santa Catarina, and northern Rio Grande do Sul States. Model projection to the Last Glacial Maximum showed practically the same potential distribution and suitable areas in the current climate. Model projection to the Last Interglacial only showed a potential expansion of suitable areas across small areas along São Paulo coast (Fig. 5B). The most important variable for *C. gouveai* was by far the Precipitation of Driest Month (Bio 14), followed by other precipitation variables (Table S6).

Niche overlap was low or zero between all pairs of groups ($D < 0.08$) and the null tests showed nonequivalence or niche similarity, indicating that all three species occupy significantly distinctive environmental niches across the exact species occurrences, as well as their respective ranges (Table 4).

Taxonomic Decisions

The data gathered from a geographically representative sample covering most of the variability in the traditional external morphological characters of the *Chironius bicarinatus* complex, in addition to the clades retrieved in molecular phylogeny and unique niches found by ecological evidence, make it possible to recognize and objectively attribute, two species with available names (*C. bicarina-*

Table 4. Results of niche overlap (D metric) and null tests of equivalence and similarity. The niche overlap was low or zero for all comparisons, and the null tests showed nonequivalence or similarity of the niches.

Species Pair	D metric	Equivalence	Similarity 1-2	Similarity 2-1
<i>C. bicarinatus</i> – <i>C. gouveai</i>	0.083	1	0.33	0.32
<i>C. bicarinatus</i> – Baturité Massif sample	0	1	0.55	0.51
Baturité Massif sample – <i>C. gouveai</i>	0	1	0.46	0.50

tus and *C. gouveai*), and diagnose a distinct lineage without an available name (Baturité Massif sample). Herein, we first redefined *C. bicarinatus*, inferring its morphological limits with *C. gouveai* and then, we formally describe the Baturité Massif sample as a new species.

Chironius bicarinatus (Wied, 1820)

Figures 6A, B, 7A, 8

Chresonymy.

Coluber bicarinatus Wied, 1820: 179; Wied (1824: Vol. 8), (1825: 284).

On a sand beach of Lagoa, near the Rio Jucú, within “5 legoas” (leagues) of Villa do Espírito Santo (currently Vila Velha), state of Espírito Santo, Brazil.

Natrix bicarinatus – Merrem (1820: 117)

Erpetodryas bicarinatus – Boie (1826: 237)

Herpetodryas bicarinatus – Wagler (1830: 180)

Herpetodryas bicarinata – Fitzinger (1843: 26)

Herpetodryas carinatus (not Linnaeus, 1758) – Schlegel (1837: 177, in part), Duméril et al. (1854: 207, in part), Jan (1863: 80, in part), Boulenger (1894: 73 [var. C], in part)

Herpetodryas carinatus var. *bicarinata* – Boettger (1898: 55, in part)

Chironius carinatus (not Linnaeus, 1758) – Amaral (1925: 4, in part)

Chironius bicarinatus – Bailey (1955: 8, in part), Peters and Orejas-Miranda (1970: 59, in part), Dixon et al. (1993: 59, in part), Entiuspe-Neto et al. (2020, in part)

Holotype. Adult male, apparently lost in the American Museum of Natural History (Vanzolini and Myers 2015) from a locality near Lagoa Grande (20°30'08.3"S, 40°21'32.4"W; ~2 m above sea level; hereafter a.s.l.), municipality of Vila Velha, state of Espírito Santo, Brazil. The data reported by Wied in the original description and in later studies (Wied 1824: color plate, Vol. 8 plate 2; 1825: 284) are adequate for the recognition of the species and its type locality, with the designation of a neotype being deemed unnecessary (ICZN 1999).

Diagnosis. *Chironius bicarinatus* is distinguished from all congeners by the following unique combination of morphological characters: (i) dorsal scale rows 12/12/10; (ii) cloacal plate divided; (iii) dorsal scale rows keeled usually two; (iv) ventrals 147–170 in females, 145–165 in males; (v) subcaudals 130–157 in females, 125–154 in males; (vi) apical pits often present only on the cervical region; (vii) three supralabials contacting orbit; (viii) temporal formula usually 1+2; (ix) after preservation, uniform olive, grayish olive or bluish dorsum with a light vertebral stripe; (x) after preservation, labials predomi-

nantly yellowish, except for the last two or three supralabials, which may present the same color of dorsal series or postocular stripe; gular region, first third of belly, and subcaudals yellowish; remainder of the belly yellowish or bluish; (xi) a medially positioned black zig-zag line between subcaudals, gradually fading to the tip of the tail; outer margins with a black outline; (xii) hemipenial body generally ornamented with papillate calyces gradually replaced by smooth calyces toward the apex; (xiii) hemipenial body with each longitudinal row presenting 14–22 spines and 5–7 spines along sulcus spermaticus; (xiv) ventral surface of the septomaxilla smooth; (xv) anteroventral surface of prefrontal lacrimal foramen smooth; (xvi) maxillary teeth 30–38; (xvii) palatine teeth 23–24; (xviii) quadrate-suspensorium articulation with posterior end of supratemporals straight.

Comparisons. *Chironius bicarinatus* differs from most congeners, except for *C. multiventris* Schmidt & Walker, 1943, *C. foveatus*, *C. septentrionalis* Dixon et al., 1993, *Chironius* cf. *exoletus*, and *C. gouveai*, by having 12/12/10 dorsal scale rows, divided cloacal plate, two keeled dorsal scale rows, presence of apical pits, and a greenish or olive dorsal pattern. *Chironius bicarinatus* differs from *C. multiventris*, *C. foveatus* and *C. septentrionalis* in its number of subcaudals 125–157 [138.7–142.0; 95% confidence intervals, hereafter] (vs. 156–208 in *C. multiventris*, 156–169 in *C. foveatus* and 165–181 in *C. septentrionalis*) and ventrals 145–170 [156.2, 157.4] (vs. 161–196 in *C. multiventris*, 163–174 in *C. foveatus* and 161–174 in *C. septentrionalis*).

The Atlantic populations of *Chironius* cf. *exoletus* (in parentheses) are the only ones that can present the aforementioned characters and a color pattern similar to *C. bicarinatus*. Specimens of *Chironius* cf. *exoletus* that have 12/12/10 dorsal scale rows are seldom observed (2% in our sample, with 12/12/8 being more frequent). Still, *C. bicarinatus* can also be differentiated by the number of maxillary teeth 30–38 [33.8–34.4] (vs. 23–31); outer margins of subcaudals pigmented black (vs. black pigmentation absent); ventral color pattern of tail usually with a black zig-zag line medially between subcaudals, gradually fading to the tip of the tail (vs. black zig-zag line maintaining the same intensity up to the tip of the tail); and hemipenial body elongated covered with more concentrated spines (vs. hemipenial body short with lower concentration of spines; see an illustration of the hemipenes in the supplementary information S1 of Klackzo et al. 2014).

Chironius bicarinatus differs from *C. gouveai* (in parentheses) in the number of ventrals 147–170 [157.0–159.0] in females and 145–165 [155.1–156.6] in males



Figure 6. General view while alive of *Chironius bicarinatus* and *Chironius gouveai*: **A** an adult of *C. bicarinatus* (MNRJ 26255) from the municipality of Rio Claro, state of Rio de Janeiro, Brazil; **B** a juvenile specimen of *C. bicarinatus* (MNRJ 27463), from the municipality of Rio de Janeiro, state of Rio de Janeiro, Brazil; **C** an adult specimen of *C. gouveai* (unvouchered specimen) from the municipality of Porto Alegre, state of Rio Grande do Sul, Brazil; **D** a juvenile specimen of *C. gouveai* (unvouchered specimen) from the municipality of Vacaria, state of Rio Grande do Sul, Brazil. Photos by M. Bilate (A), F. Dias-Silva (B), M. Borges-Martins (C), and O.L. Balbinot (D).

(vs. 156–174 [162.8–164.8] in females and 151–167 [157.9–159.3] in males); maxillary teeth 30–38 [33.8–34.4] (vs. 27–36 [30.5–31.4]); color pattern in preservative with uniformly olive, grayish olive or bluish dorsum and a black zig-zag line medially between subcaudals, gradually fading to the tip of tail (vs. dorsum usually uniform light brown, grayish olive or bluish, and dorsal and ventral scales with black or brown edges without a zig-zag line; see Entiauspe-Neto et al. 2020: fig. 3 for an illustration of this character); temporal formula usually 1+2 (vs. 1+1); ventral surface of septomaxilla smooth (vs. presence of a conspicuous projection); anteroventral surface of prefrontal lacrimal foramen smooth (vs. presence of a conspicuous projection); and posterior end of supratemporals straight (vs. slightly laterally curved).

Color pattern variation in preservative. Adult specimens with uniformly olive, grayish olive or bluish dorsum and light vertebral and postocular stripes that may or may not be evident, sometimes with black outer margins bordering it, more visible on the anterior part of the body. Predominantly pale yellowish labials, except for the last two or three supralabials, which may present the same dorsal or postocular stripe color. Ventrally, gular region, first third of the belly, and subcaudals pale yellowish; the

remainder of the belly pale yellowish or bluish. Most have outer subcaudal margins with a black outline and a medially positioned black zig-zag line between subcaudals (gradually fading to the tip of the tail), which may vary in intensity and may even be absent in some specimens. Juvenile specimens have the same color pattern variation as adults, but they can also have a uniform olive brown dorsum and light crossbands on dorsum. In our sample, the presence of light crossbands on dorsum was found in juvenile specimens with a maximum SVL of 373 mm (CHUFJF 523) and in only one adult specimen (MNRJ 1839, SVL 830 mm), collected in the municipality of Passa Quatro, state of Minas Gerais, Brazil.

Color pattern while alive (Fig. 6A, B). The description of color pattern while alive is based on photographs of six adult specimens (MNRJ 19138, 22017, 23571, 24194, 24877, 26255), and a juvenile specimen (MNRJ 27463), all collected in several localities of the state of Rio de Janeiro, Brazil; as well as on photographic material of other unvouchered specimens (iNaturalist, $n = 9$; see Appendix 2). Adult specimens have a uniformly green, olive or grayish olive dorsum with a light vertebral, sometimes with black outer margins bordering it, more visible on the anterior part of the body, and a black postocular

stripe. Predominantly yellowish supralabials, except for the last two or three, which may present the same dorsal or postocular stripe color. Infralabials and gular region mostly whitish or yellowish; the first third of belly and subcaudals yellowish; the remainder of the belly whitish yellow. As in preserved specimens, while alive juvenile specimens also have a uniform olive brown dorsum and light crossbands on dorsum.

Hemipenial morphology (Fig. 7A). We analyzed the hemipenes of 23 specimens of *Chironius bicarinatus*, five of which were extracted from the specimens and manually fully everted, rendering almost or virtually maximally expanded organs. The description of hemipenes is based on the fully everted and maximally expanded left organs of the specimens MNRJ 4008, 25558, and also on the partially expanded organs of specimens MNRJ 8717, 25434; and the maximally expanded right organ of the specimen MNRJ 18909. Hemipenis unilobed, unicalyculate, non-capitate; subcylindrical shape, with a simple sulcus spermaticus, running centripetally from the base to the apex (MNRJ 4008) or slightly more than half of the hemipenis (MNRJ 25434); apex may present a nude area (MNRJ 25558) or may not (MNRJ 18909), generally with papillate calyces, but can also present calyces with few papillae on the apex and medial region (MNRJ 18909, 25558); each longitudinal row presenting 21–29 calyces; the calyces towards the hemipenial body are replaced by spinulate calyces; hemipenial body represents more than half of the total length of the organ, and is covered in spines that gradually increase in size toward the base, reaching maximum size at just over half of hemipenial body; each longitudinal row presenting 14–22 spines and 5–7 spines along sulcus; base mostly nude, ornamented by spinules at the upper portion and also laterally distributed on the proximal region of sulcus spermaticus; a basal naked pocket is present on the medial region.

Distribution (Fig. 8). *Chironius bicarinatus* is distributed in the Ombrophilous Dense and Semideciduous Forests along the coast, from the São Francisco River, state of Sergipe, Northeastern Brazil (northernmost record in the municipality of Capela; 10°32'S, 37°03'W), to the Serra do Tabuleiro, state of Santa Catarina, Southern Brazil (southernmost record in the municipality of Florianópolis; 27°35'38.5"S, 48°32'54.0"W) between sea level to ~930 m a.s.l..

Remarks. The records of *Chironius bicarinatus* (ZVC 1336, MNHN 3924) in Montevideo, Uruguay, can be explained by the accidental introduction of specimens into the agricultural market of Montevideo by banana shipments from the state of São Paulo, Brazil (Carreira and Maneyro 2013). Strangely, two records of *C. bicarinatus* (CHUFC 3604, MZFS 1279) were reported from the municipalities of Mulungu and Juazeiro, respectively in the states of Ceará and Bahia. Similarly, we believe it is more likely that these records are also due to accidental introduction by banana shipments from the Bahia coastal region than that the representation of small, well-established



Figure 7. Hemipenial morphology of *Chironius bicarinatus* and *Chironius gouveai*: **A** asulcate (left) and sulcate (right) views of the hemipenis of *C. bicarinatus* (MNRJ 25558) from the municipality of Petrópolis, state of Rio de Janeiro, Brazil; **B** asulcate (left) and sulcate (right) views of the hemipenis of *C. gouveai* (MHNCI 12369) from the municipality of Candói, state of Paraná, Brazil. Scale bar = 5 mm.

populations above the São Francisco River. Possible evidence of this would be the northernmost records of *C. bicarinatus* (NMB 1303, 1304) reported by Dixon et al. (1993), further inland in the state of Bahia, municipality of Andaraí. We verified these records in the Institution's catalog, which contained the following data: "BRA Bahia Andarahy pequeno > Andahary pequeno" donated by "Massini, Hans, Rio de Janeiro". Thus, we can conclude that it is more likely that these records are from a location in the state of Rio de Janeiro, known as Tijuca (formerly known as Andaraí Pequeno), since the donor was a resident of this neighborhood.

Chironius gouveai Entiauspe-Neto et al., 2020

Figures 6C, D, 7B, 8

Chresonymy.

Chironius bicarinatus – Bailey (1955: 8, in part), Orejas-Miranda (1958: 1), Peters and Orejas-Miranda (1970: 59, in part), Williams

and Francini (1991: 63), Cei (1993: 538), Dixon et al. (1993: 59, in part), Achaval and Olmos (1997: 68), Giraudo (2001: 42), Carreira et al. (2005: 267), Carreira and Maneyro (2013: 148), Entiauspe-Neto et al. (2020, in part)

Holotype. Adult male, CHFURG 4394, from municipality of Tapes (30°28'46.7"S, 51°23'46.1"W; ~74 m a.s.l.), state of Rio Grande do Sul, Brazil. The holotype was not examined first-hand, but its identity has been confirmed through the information present in the original description (Entiauspe-Neto et al. 2020).

Paratypes. Seven specimens, all from the state of Rio Grande do Sul, Brazil: Adult male, ZUFMS 2908, from the municipality of Bagé; adult male, ZFMK 103132 (formerly CHFURG 1504), from the municipality of Rio Grande; adult female, MCP 2631, at Rodeio Bonito, municipality of São Francisco de Paula; adult male and female, respectively, CHFURG 4823–24, at Ilha da Torotama, municipality of Rio Grande; adult male, MCP 8968, at Gomercinda Dornelles Fountoura School, municipality of Encruzilhada do Sul; adult male, MCP 12762, municipality of Triunfo (Entiauspe-Neto et al. 2020). Only the specimen MCP 8968 was examined first-hand.

Diagnosis. *Chironius gouveai* is distinguished from all congeners by the following unique combination of morphological characters: (i) dorsal scale rows 12/12/10; (ii) cloacal plate divided; (iii) dorsal scale rows keeled usually two; (iv) ventrals 156–174 in females, 151–167 in males; (v) subcaudals 139–146 in females, 131–152 in males; (vi) apical pits often present only on the cervical region; (vii) three supralabials contacting orbit; (viii) temporal formula usually 1+1; (ix) after preservation, uniform light brown, grayish olive or bluish dorsum with a light vertebral stripe; and dorsals and ventrals with black or brown edges; (x) after preservation, labials predominantly yellowish or whitish, except for the last two or three supralabials, which may present the same color of dorsal series or postocular stripe; gular region, first third of belly, and subcaudals (which can also be whitish) yellowish; remainder of the belly can be yellowish, olive or bluish; (xi) subcaudals with black or brown edges; outer margins with a black outline; (xii) hemipenial body generally ornamented with papillate calyces gradually replaced by smooth calyces toward the apex; (xiii) hemipenial body with each longitudinal row presenting 14–19 spines and 5–6 spines along sulcus spermaticus; (xiv) ventral surface of the septomaxilla with a conspicuous projection; (xv) anteroventral surface of prefrontal lacrimal foramen with a conspicuous projection; (xvi) maxillary teeth 27–36; (xvii) palatine teeth 16–18; (xviii) quadrate-suspensorium articulation with posterior end of supratemporals slightly laterally curved.

Comparisons. *Chironius gouveai* differs from most congeners, except for *C. multiventris*, *C. foveatus*, *C. septentrionalis*, *Chironius* cf. *exoletus*, and *C. bicarinatus*, by having 12/12/10 dorsal scale rows, divided cloacal plate, two keeled dorsal scale rows, presence of apical pits, and

a greenish or olive dorsal pattern. *Chironius gouveai* differs from *C. multiventris*, *C. foveatus* and *C. septentrionalis* in its number of subcaudals 131–152 [139.8–142.9; 95% confidence intervals] (vs. 156–208 in *C. multiventris*, 156–169 in *C. foveatus* and 165–181 in *C. septentrionalis*) and ventrals 151–174 [160.1–161.5] (vs. 161–196 in *C. multiventris*, 163–174 in *C. foveatus* and 161–174 in *C. septentrionalis*).

Chironius gouveai differs from *Chironius* cf. *exoletus* (in parentheses) in terms of number of maxillary teeth 27–36 [30.5–31.4] (vs. 23–31); outer margins of subcaudals with black pigmentation (vs. black pigmentation absent); ventral color pattern of tail usually with black or brown edges without a black zig-zag line medially (vs. a black zig-zag line medially between subcaudals); and hemipenial body elongated covered with more concentrated spines (vs. hemipenial body short with lower concentration of spines; see an illustration of the hemipenes in Klackzo et al. 2014).

Chironius gouveai differs from *C. bicarinatus* (in parentheses) in the number of ventrals 156–174 [162.8–164.8] in females and 151–167 [157.9–159.3] in males (vs. 147–170 [157.0–159.0] in females and 145–165 [155.1–156.6] in males); maxillary teeth 27–36 [30.5–31.4] (vs. 30–38 [33.8–34.4]); color pattern in preservative with dorsum usually uniform light brown, grayish olive or bluish, and dorsal and ventral scales with black or brown edges without a zig-zag line (vs. uniformly olive, grayish olive or bluish dorsum and a black zig-zag line medially between subcaudals, gradually fading to the tip of tail; see Entiauspe-Neto et al. 2020: fig. 3 for an illustration of this character); temporal formula usually 1+1 (vs. 1+2); ventral surface of septomaxilla with a conspicuous projection (vs. septomaxilla smooth); anteroventral surface of prefrontal lacrimal foramen with a conspicuous projection (vs. anteroventral surface of lacrimal foramen smooth); and posterior end of supratemporals slightly laterally curved (vs. straight).

Color pattern variation in preservative. Most adult specimens have a uniform light brown, grayish olive or bluish dorsum with a light vertebral stripe, that may or may not be evident, depending on the preserved condition, sometimes with black outer margins bordering it, more visible on the anterior part of the body. It is also possible to notice the presence of a black postocular stripe in better preserved specimens. Dorsals and ventrals with black or brown edges, more visible on the posterior part of the belly. Predominantly pale yellowish or whitish labials, except for the last two or three supralabials, which may present the same dorsal or postocular stripe color. Gular region, first third of belly, and subcaudals (which can also be whitish) pale yellowish; the remainder of the belly pale yellowish, olive or bluish. The outer margins of subcaudals have a black outline, which may vary in intensity and may even be absent in some specimens, and subcaudals have black or brown edges. Some specimens have remnants of black edges on subcaudals and only medially positioned black zig-zag line between subcaudals is evident.

The populations near Serra do Mar, in the states of Paraná and Santa Catarina (e.g., FML 1816, CHUFSC 244, 625, 788–90, 898, 1035, 1105, 2976–77), have a color pattern that is more similar to *C. bicarinatus* than those that occur in further inland locations. As with the *C. bicarinatus* specimens, they have a uniform olive or grayish olive dorsum; Gular region, first third of the belly, and subcaudals pale yellowish; the remainder of the belly pale yellowish or bluish; no black or brown edges on dorsals and ventrals; and the only distinguishable feature would be an evident black zig-zag line medially positioned between subcaudals with more intensity compared to *C. bicarinatus*, also gradually fading to the tip of the tail.

Juvenile specimens have the same color pattern variation as adults and juvenile specimens of *C. bicarinatus*, differing in the greater intensity of the black zig-zag line medially positioned between subcaudals or in the remnants of black or brown edges on dorsals and ventrals; neither may be evident in some preserved specimens, and it is therefore, only possible to distinguish juveniles of the related species by the combination of some meristic characters (e.g., temporal formula, number of subcaudals or maxillary teeth).

Color pattern while alive (Fig. 6C, D). The description of color pattern while alive is based on photographs of an adult specimen (MACN 38879) collected in the province of Misiones, Argentina; a juvenile specimen (unvouchered specimen) from the municipality of Vacaria, state of Rio Grande do Sul, Brazil, as well as on photographic material of other unvouchered specimens (iNaturalist, n = 9; see Appendix 2).

Adult specimens with uniform light brown, grayish olive or olive dorsum and a light vertebral stripe, sometimes with black outer margins bordering it, more visible on the anterior part of the body. Dorsals and ventrals with black edges, more visible on the posterior part of the belly. Predominantly yellowish or whitish supralabials, except for the last two or three, which may present the same dorsal or postocular stripe color. Infralabials and gular region mostly yellowish or whitish; the first third of the belly (can also be whitish) and subcaudals yellowish or brownish yellow; the remainder of the belly whitish yellow or brownish yellow. For most specimens, the outer margins of subcaudals have a black outline and subcaudals have black edges.

Hemipenial morphology (Fig. 7B). We analyzed the hemipenes of 19 specimens, 13 of which were extracted from the specimens and prepared, rendering a fully everted and almost or virtually maximally expanded organs. The description is based on the fully everted and maximally expanded left organs of the specimens MCP 17282, MHNCI 12369, UFMT 1600, partially expanded organ of the specimen MHNCI 1529, and non-maximally expanded organs of the specimens MHNCI 7134, ZVC 2041, ZVC 3681; and on the fully everted and maximally expanded right organ of the specimen MCP 2423, and partially expanded organs of the specimens MCN 3144, MCN 14090. Retracted organs extend to the level of the twelfth subcaudal (n = 3).

Hemipenis unilobed, unicalyculate, noncapitate, subcylindrical shape, with a simple sulcus spermaticus, running centripetally from the base to the apex (MCN 3144) or slightly more than half of the hemipenis (MHNCI 12369, UFMT 1600); no nude area on the apex, ornamented with papillate calyces in the sulcate side and with spinulate calyces in the middle of the asulcate side; hemipenis eventually showing calyces with few papillae on the apex and medial region (MHNCI 12369, UFMT 1600); each longitudinal row presenting 24–27 calyces; calyces towards hemipenial body replaced by spinulate calyces; hemipenial body with approximately more than half of the total length of the organ, and is covered in spines that gradually increase in size towards the base, reaching maximum size at just over half of the hemipenial body; with each longitudinal row presenting 14–19 spines and 5–6 spines along the sulcus spermaticus; base mostly nude, ornamented by spinules at the upper portion and also laterally distributed on the proximal region of the sulcus spermaticus; a basal naked pocket present on the medial region.

Distribution (Fig. 8). *Chironius gouveai* is widely distributed across inland Serra do Mar at higher altitudes in the Mixed and Semideciduous Forests, from the Paranapanema River (northernmost record in the municipality of Londrina; 23°18'34.6"S, 51°10'26.4"W) to the Uruguayan pampas (southernmost record in the province of Río Negro, M'Bopigua Port; 33°06'38.7"S, 58°11'31.6"W), with its western limit by the Paraná River (westernmost record in the province of Corrientes, Itá Ibaté, Argentina; 27°25'43.8"S, 57°20'17.0"W), between sea level to ~1030 m a.s.l..

Remarks. The records of *Chironius gouveai* (ZVC 2041, 2956, 3681, 3727, MNHN 78, 1730, 1794, 5707) in the departments of Artigas, Río Negro and Salto, western Uruguay, can be explained by the attempt of specimens to cross the Uruguay River and their transportation by vegetation rafts along the river bed to the La Plata River (see Achaval et al. 1979). The record of *C. gouveai* (MHNCI 6028) from Montevideo needs to be clarified to confirm the occurrence of the species in southern Uruguay.

Chironius dracomaris sp. nov.

<https://zoobank.org/E0F5FBF9-C031-4999-B952-7E1F42893B22>

Figures 8–13

Chresonymy.

Chironius carinatus carinatus – Dixon et al. (1993: 73 [MZUSP 3633], in part)

Chironius bicarinatus – Borges-Nojosa (2007: 236), Guedes et al. (2014: 27, in part), Roberto and Loebmann (2016: 142), Entiauspe-Neto et al. (2020: 102, in part)

Holotype. Adult male, MNRJ 27716 (formerly CHUFSC 3304), collected by Clécio Aragão on January 11, 1998

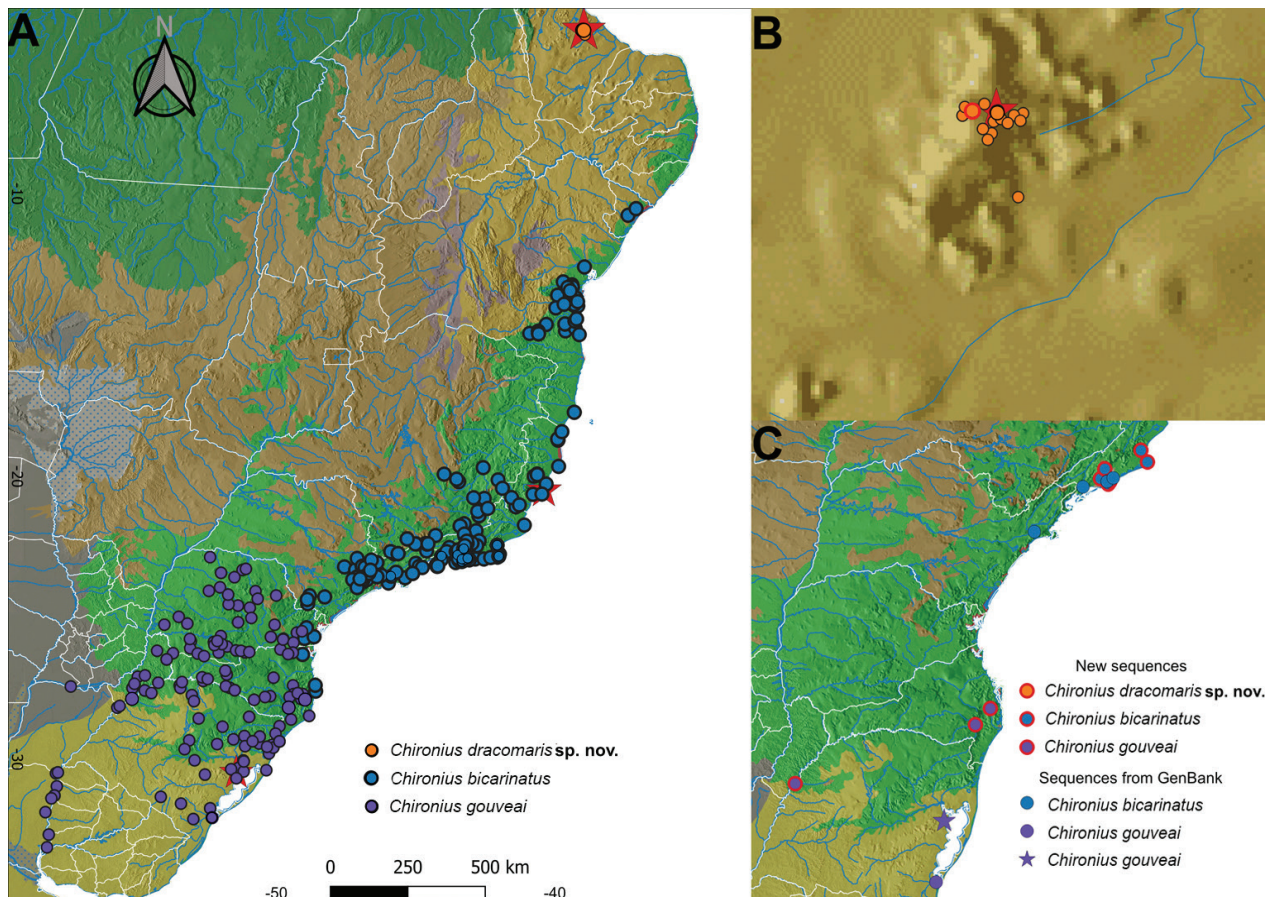


Figure 8. Distribution of the *Chironius bicarinatus* complex (A), based on first-hand examined and photographic records with locality data: *C. bicarinatus*: blue circles; *C. gouveai*: purple circles; *C. dracomaris* sp. nov.: orange circles. The stars represent their respective type localities; **B** zoomed map of the Baturité Massif, an area of distribution of *Chironius dracomaris* sp. nov.; **B, C** zoomed maps of molecular sampling localities, with the new sequences obtained in this study (highlighted in red) and sequences selected from GenBank.

at Horto Florestal ($4^{\circ}13'23.9''\text{S}$, $38^{\circ}55'28.1''\text{W}$; ~ 800 m a.s.l.), Granja neighborhood, municipality of Pacoti, state of Ceará, Brazil.

Paratypes. Seventeen specimens, all from Baturité Massif, state of Ceará, Brazil: juvenile female, CHUFC 1389, collected by P. Cascon on April 27, 1989 at Mata do Remanso ($4^{\circ}14'34.1''\text{S}$, $38^{\circ}55'46.6''\text{W}$), municipality of Guaramiranga; adult female, CHUFC 1414, collected by R. Otoch on September 28, 1989 at Sítio Abreu ($4^{\circ}15'23.3''\text{S}$, $38^{\circ}56'59.7''\text{W}$), municipality of Guaramiranga; adult female, CHUFC 2383, collected by D.M. Borges-Nojosa on January 28, 2000 in the municipality of Pacoti; adult male, CHUFC 2747, collected by D.M. Borges-Nojosa on November 02, 1997 at Sítio Olho D'Água dos Tangarás ($4^{\circ}14'16.4''\text{S}$, $38^{\circ}54'56.7''\text{W}$), municipality of Pacoti; adult male, CHUFC 2751, collected by D.M. Borges-Nojosa on August 15, 1998 at Horto Florestal, Granja ($4^{\circ}13'23.9''\text{S}$, $38^{\circ}55'28.1''\text{W}$), municipality of Pacoti; adult female, CHUFC 2759, collected by D.M. Borges-Nojosa on January 11, 1998 at Horto Florestal, Granja, municipality of Pacoti; adult female, CHUFC 2840, collected by W.C. Luz on June 27, 2006 in the municipality of Pacoti; adult female, CHUFC 3305, collected by C. Aragão on December

16, 1997 at Linha da Serra community ($4^{\circ}13'53.8''\text{S}$, $38^{\circ}59'18.7''\text{W}$), municipality of Guaramiranga; adult male, CHUFPB 17304, from APA da Serra de Baturité ($4^{\circ}16'35.7''\text{S}$, $38^{\circ}56'26.7''\text{W}$), municipality of Guaramiranga; adult male, FUNED 1012, collected by E.O. Barros on May 22, 1988 at Sítio Macapá ($4^{\circ}15'53''\text{S}$, $38^{\circ}56'0.1''\text{W}$), municipality of Guaramiranga; adult female, MHNCE-R 59, collected by D.C. Lima on October 18, 2019 at Museu de História Natural do Ceará Prof. Dias da Rocha ($4^{\circ}13'35.5''\text{S}$, $38^{\circ}55'21.9''\text{W}$), municipality of Pacoti; adult female, MNRJ 27803, collected by S.V. Mendonça and L. Tavares on November 28, 2020 at Museu de História Natural do Ceará Prof. Dias da Rocha; adult male, MNRJ 27804, collected by T. Cavalcante, L. Lima, V.L.M. Rodrigues and L. Silva on May 29, 2022 at Pernambucozinho ($4^{\circ}13'21.6''\text{S}$, $38^{\circ}58'10.9''\text{W}$), municipality of Guaramiranga; subadult female, MHNCE-R 577, collected by J.A. Oliveira on July 18, 2022 at Museu de História Natural do Ceará Prof. Dias da Rocha; adult male, MHNCE-R 616, collected by J.A. Oliveira on November 30, 2022 at Museu de História Natural do Ceará Prof. Dias da Rocha; adult male, MNRJ 27717, collected by D.M. Borges-Nojosa on January 03, 1999 at Sítio Olho D'Água dos Tangarás, municipality of Pacoti; adult male, MNRJ 27718, collected by C. Aragão on

December 18, 1997 at Sítio Pau D'Alho (4°13'32.2"S, 38°55'34.8"W), municipality of Pacoti.

Diagnosis. *Chironius dracomaris* can be distinguished from all congeners by the following unique combination of morphological characters: (i) dorsal scale rows 12/12/10; (ii) cloacal plate divided; (iii) two or more keeled dorsal scale rows (2nd–11th dorsal rows); (iv) ventrals 154–162 in females, 149–159 in males; (v) subcaudals 124–135 in females, 132–138 in males; (vi) apical pits present on the cervical and in at least one other region of the body (paravertebral rows, cloacal region, and/or tail); (vii) three or two supralabials contacting orbit; (viii) temporal formula usually 1+2; (ix) after preservation, uniform grayish olive or bluish dorsum with a light vertebral stripe and two black stripes visible from neck to midbody; (x) after preservation, the snout (rostral, nasals and internasals) can be light brown or have the same dorsal color; labials predominantly whitish, except for the last two supralabials, which may present the same color of dorsal series or postocular stripe; gular region, first third of belly, near cloacal region and subcaudals whitish; remainder of the belly olive or bluish; (xi) subcaudals have slightly black edges; (xii) hemipenial body generally ornamented with papillate calyces gradually replaced by a small concentration of smooth calyces on the proximal region at the end of the sulcus spermaticus; (xiii) each longitudinal row of hemipenial body has 15–22 spines and 5–8 spines along sulcus spermaticus; (xiv) ventral surface of the septomaxilla smooth; (xv) anteroventral surface of prefrontal lacrimal foramen smooth; (xvi) 34–39 maxillary teeth; (xvii) palatine teeth 24; (xviii) quadrate-suspensorium articulation with posterior end of supratemporals straight.

Comparisons. The new species differs from most congeners, except for *Chironius bicarinatus*, *C. gouveai*, *C. multiventris*, *C. foveatus*, and *C. septentrionalis*, by having 12/12/10 dorsal scale rows, divided cloacal plate, two or more keeled dorsal scale rows, the presence of apical pits, and a greenish or olive dorsal pattern. Regarding the species of the *C. multiventris* complex (*C. multiventris*, *C. foveatus*, and *C. septentrionalis*), *Chironius dracomaris* can be easily distinguished by the number of subcaudals 124–138 [129.1–132.2; 95% confidence intervals] (vs. 156–208 in *C. multiventris*, 156–169 in *C. foveatus* and 165–181 in *C. septentrionalis*) and ventrals 149–162 [154.7–156.1] (vs. 161–196 in *C. multiventris*, 163–174 in *C. foveatus* and 161–174 in *C. septentrionalis*).

Chironius dracomaris differs from *C. gouveai* (in parentheses) in the number of subcaudals 124–135 [127.7–130.9] in females and 132–138 [131.3–136.0] in males (vs. 139–146 [140.2–143.4] females and 131–152 [139.1–143.4] males); maxillary teeth 34–39 [35.3–36.0] (vs. 27–36 [30.5–31.4]); temporals usually 1+2 (vs. 1+1); apical pits present on the cervical and in at least one other region of the body [e.g., paravertebral rows, cloacal region, and/or tail] (vs. usually only on the neck); color pattern in preservative: uniform grayish olive or bluish dorsum and two black dorsolateral stripes visible from neck to midbody (vs. usually a uniform light brown, gray-

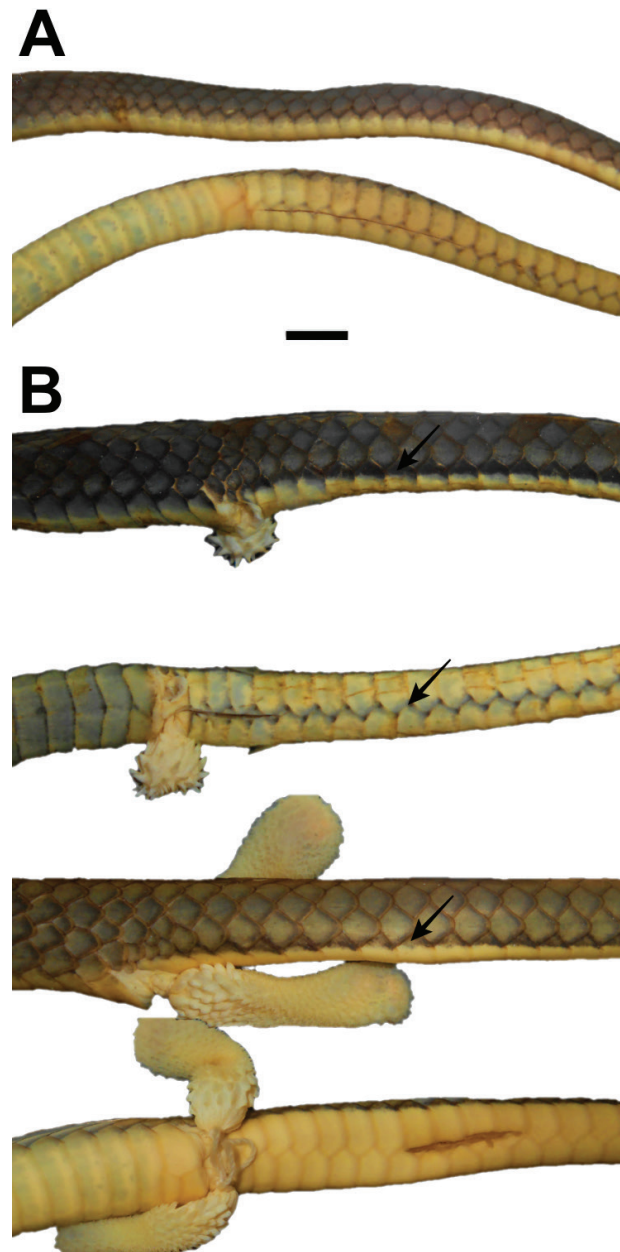


Figure 9. Color pattern of subcaudal scales comparing (A) *Chironius dracomaris* sp. nov. (MNRJ 27716, holotype) and (B) *C. bicarinatus* (MNRJ 25434, 14983). Arrows indicate a medially positioned black zig-zag line between subcaudals (ventral view) and outer margins with a black outline (lateral view). See Table 5 for detailed comparisons of the most frequent qualitative diagnostic characters. Scale bar = 10 mm.

ish olive or bluish dorsum; dorsal and ventral scales with black or brown edges); subcaudals with slightly black edges, outer margins without a black outline or a black zig-zag line medially positioned between subcaudals (vs. outer margins with a black outline and subcaudals with black or brown edges; see Fig. 9 and Entiauspé-Neto et al. 2020: fig. 3 for an illustration of this character); ventral surface of the septomaxilla smooth (vs. presence of conspicuous projection); anteroventral surface of prefrontal lacrimal foramen smooth (vs. presence of a conspicuous projection); and posterior end of supratemporals straight (vs. slightly laterally curved).



Figure 10. Dorsal and ventral views of the whole specimen (A); detailed dorsal, ventral (B), and lateral (C) views of head of the holotype of *Chironius dracomaris* sp. nov. (MNRJ 27716, male, SVL 652 mm) from Horto Florestal, Granja neighborhood, municipality of Pacoti, state of Ceará, Brazil. Scale bar = 5 mm.

Chironius dracomaris differs from *C. bicarinatus* (in parentheses), in the number of subcaudals 124–135 [127.7–130.9] in females and 132–138 [131.3–136.0] in males (vs. 130–157 [137.8–142.9] in females and 125–154 [138.1–142.6] in males); maxillary teeth 34–39 [35.3–36.0] (vs. 30–38 [33.8–34.4]); color pattern in preservative: uniform grayish olive or bluish dorsum and two black dorsolateral stripes visible from neck to midbody (vs. a uniform olive, grayish olive or bluish dorsum); and subcaudals with slightly black edges, outer margins without a black outline or a black zig-zag line medially positioned between subcaudals (vs. outer margins with a black outline and a medially positioned black zig-zag line between subcaudals, gradually fading to the tip of the tail; see Fig. 9).

Description of the holotype (Figs 10, 11). SVL 652 mm; midbody diameter 13.88 mm (2.1% SVL); CL 332 mm (tail tip broken); head distinct from the neck; head length 19.26 mm (2.9% SVL); head width 10.25 mm (53.2% head length); head height 9.11 mm. Head arched in lateral view; snout rounded in dorsal view; canthus rostralis slightly defined. Interocular distance 8.30 mm; snout width (at loreals level) 6.68 mm; distance between nostrils 4.99 mm; snout length 7.53 mm; nostril-orbit distance 4.31 mm; rostral subtriangular, twice as long as high, 2.05 mm high, 4.32 mm wide, slightly visible in dorsal view; internasal 2.7 mm long, 2.7 mm wide, in frontal view, internasal suture slightly straight with respect to prefrontal suture; prefrontal 3.2 mm long, 3.9 mm wide; supraocular subtrapezoidal, 6.8 mm long, 2.9 mm wide; frontal

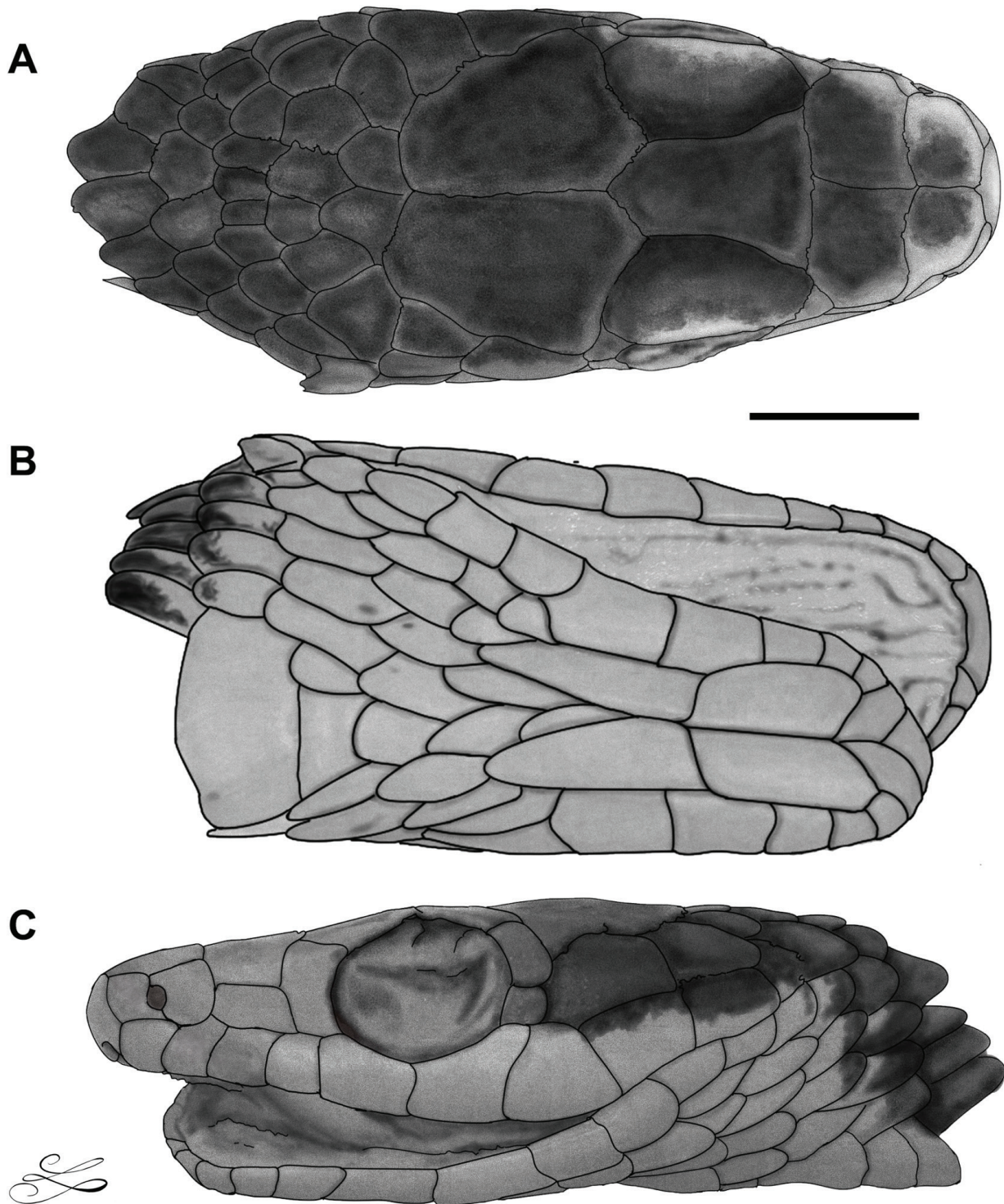


Figure 11. Dorsal (A), ventral (B), and lateral (C) views of the head of the holotype of *Chironius dracomaris* sp. nov. (MNRJ 27716) from Horto Florestal, Granja neighborhood, municipality of Pacoti, state of Ceará, Brazil. Scale bar = 5 mm.

subpentagonal, 6.4 mm long, 4.5 mm wide; parietal 8.1 mm long, 5.2 mm wide; nasal divided, nostril restricted to anterior nasal; anterior nasal 2.4 mm long, 1.7 mm high; posterior nasal 1.2 mm long, 1.7 mm high; loreal longer than higher (2.2 x 1.2 mm); second and third supralabial contacting loreal; preocular (1.5 mm long, 3 mm high); orbit diameter 5.6 mm; pupil rounded; two postoculars, the upper one higher than the lower (2.1 x 1.3 mm); temporals 1+2 (1+1 on the left side); anterior temporal 3.9 mm long, 2.6 mm high; anterior temporal in contact with

parietal, postoculars, and seventh–ninth supralabial; upper posterior temporal higher than lower posterior temporal; upper posterior temporal 2.7 mm long, 1.9 mm high; lower posterior temporal 2.7 mm long, 1.3 mm high; supralabials 9, fifth–sixth with orbit; first to third supralabial similar in size and higher than fourth supralabial (longer than first supralabial); the remaining supralabial (fifth–ninth) longer and higher than first four supralabials; symphyisial triangular; infralabials 10, first five infralabials contacting the first pair of chinshields and fifth–sixth with

the second one; the first pair of chinshields 5 mm long, 2.3 mm wide; the second pair of chinshields 6.8 mm long, 2 mm wide; ventrals 152; subcaudals 127/127 (tail tip broken); cloacal plate divided; dorsal scale in 12/12/10 rows; the anterior part of the body has two rows of keeled dorsal scales (6th, 7th) with low intensity on neck region and remnants of keeled scales (2nd–11th dorsal rows), which increase in intensity towards midbody; in the midbody, all scales (2nd–11th dorsal rows) have a strong keel intensity; in the posterior region up to the cloaca, there are remnants of keeled scales (1st, 12th dorsal rows), some weak keeled scales (2nd–9th dorsal rows), and the paravertebral rows (6th, 7th) still with strong intensity, being the only keeled rows that reach the tail; apical pits on the neck, paravertebral rows and tail; maxillary teeth 35/34.

Uniform grayish olive dorsum with a light vertebral stripe and two black dorsolateral stripes on each side visible from neck to midbody (until the 75th ventral); presence of a black postocular stripe; snout (rostral, nasals and internasals) light brown; predominantly whitish labials, except for the last supralabial, which presents the same postocular stripe color. Gular region, the first third of the belly, near cloacal region and subcaudals whitish; the remainder of the belly olive; subcaudals with slightly black edges.

Color pattern variation in preservative. Adult specimens have a uniform bluish dorsum with a light vertebral stripe and two dorsolateral black stripes, laterally visible from neck to midbody, which may or may not be evident, depending on the preserved condition, as well as the presence of a black postocular stripe. The snout can have the same dorsal color; predominantly whitish labials, except for the last two supralabials, which may present the same dorsal or postocular stripe color. Gular region, the first third of the belly, near cloacal region and subcaudals whitish; the remainder of the belly may be bluish. Juvenile specimens have the same color pattern variation present in adults, but they have a uniform olive brown dorsum and light crossbands along the dorsum. In our sample, the presence of light crossbands on the dorsum was found in juvenile specimens with a maximum SVL of 257 mm (CHUFC 3226) from Sítio São José, Pacoti, Ceará.

Color pattern while alive (Fig. 12). The description of color pattern while alive is based on photographs of adult specimens MNRJ 27803 and MHNCE-R 577 from Pacoti and IBSP 76994 or 76995 from Sítio Álvaro, Guaramiranga, both in Ceará state. The latter specimens were destroyed in a fire on May 15, 2010, only leaving photographic material of one of the specimens while alive. Adult specimens of *Chironius dracomaris* have a uniform green or olive dorsum; snout and first supralabials without contact with the orbit light brown; other labial scales and gular region whitish; the first third of the belly, near cloacal region and subcaudals yellowish; the remainder of the belly greenish.

Hemipenial morphology (Fig. 13A). Based on the fully everted and maximally expanded left organ of the

specimens MNRJ 27717 and MNRJ 27804, partially expanded organ of the specimen MNRJ 27718; and on the fully everted and maximally expanded right organ of the specimen MNRJ 27716, and partially everted organ of the specimen CHUFPB 17304 (n = 5). Retracted organs extend to level of eighth or ninth subcaudal (n = 3). Hemipenis unilobed, unicalyculate, noncapitate, subcylindrical shape, with a simple sulcus spermaticus, running centripetally from the base to slightly more than half of the hemipenis, not reaching the apex (MNRJ 27717); no nude area on the apex, which is ornamented with papillate calyces on the sulcate side and with spinulate calyces in the middle of the asulcate side; hemipenis also presenting calyces with few papillae on proximal region of the end of sulcus; each longitudinal row has 23–29 calyces; calyces towards hemipenial body replaced by spinulate calyces; hemipenial body represents approximately more than half of the total length of the organ, and is covered in spines that gradually increase in size toward the base, reaching maximum size at just over half of the body; each longitudinal row has 15–22 spines and 5–8 spines along sulcus spermaticus; base mostly nude, ornamented by spinules on the upper portion and also laterally distributed on the proximal region of sulcus spermaticus; a basal naked pocket present on the medial region.

Cranial osteology (Fig. 3G–I, P–R). The description of the skull of *Chironius dracomaris* is based on a scanned specimen MNRJ 27717 (paratype, SVL 680 mm). **Snout Complex.** **Premaxilla:** subtriangular in frontal view, with the ascending process oriented posterodorsally without contacting anterior end of nasals; in lateral view, anterior edge of the ascending process straight; transverse process elongated and projected laterally, slightly shorter than ascending process (sensu Klaczko et al. 2014); in ventral view, vomerine processes long (sensu Klaczko et al. 2014), posteriorly oriented, does not contact anterior end of vomers; **septomaxillae:** strongly convex dorso-medially, with long ascending conchal process extending anterolaterally, does not reach the ends of nasals; slightly separated from each other; prominent projection on the posterolateral edge of vomeronasal cupola of the septomaxilla, approaching frontals posteriorly, one side in contact with the frontal and the other slightly separated; posterior portion contacts vomers ventrally; absence of a conspicuous extension in the medial portion of septomaxilla ventrally oriented; **nasals:** in contact medially, with anterior processes tapered; no contact with premaxilla; oval anterolateral processes (sensu Klaczko et al. 2014); posterior processes almost contact anterior part of frontals; vertical lamina do not contact septomaxillae; **vomers:** with globular mesoventral portion with rounded opening corresponding to exochoanal fenestra; in this region, vomers approach medially and almost contact anterior region of the palatine laterally; large vertical posteromedial laminae with a large circular fenestra; also presents foramina in vertical laminae in the antero and mesoposterior portions; vomeronasal cupola with a tapered process projected posterodorsally above circular fenestra.

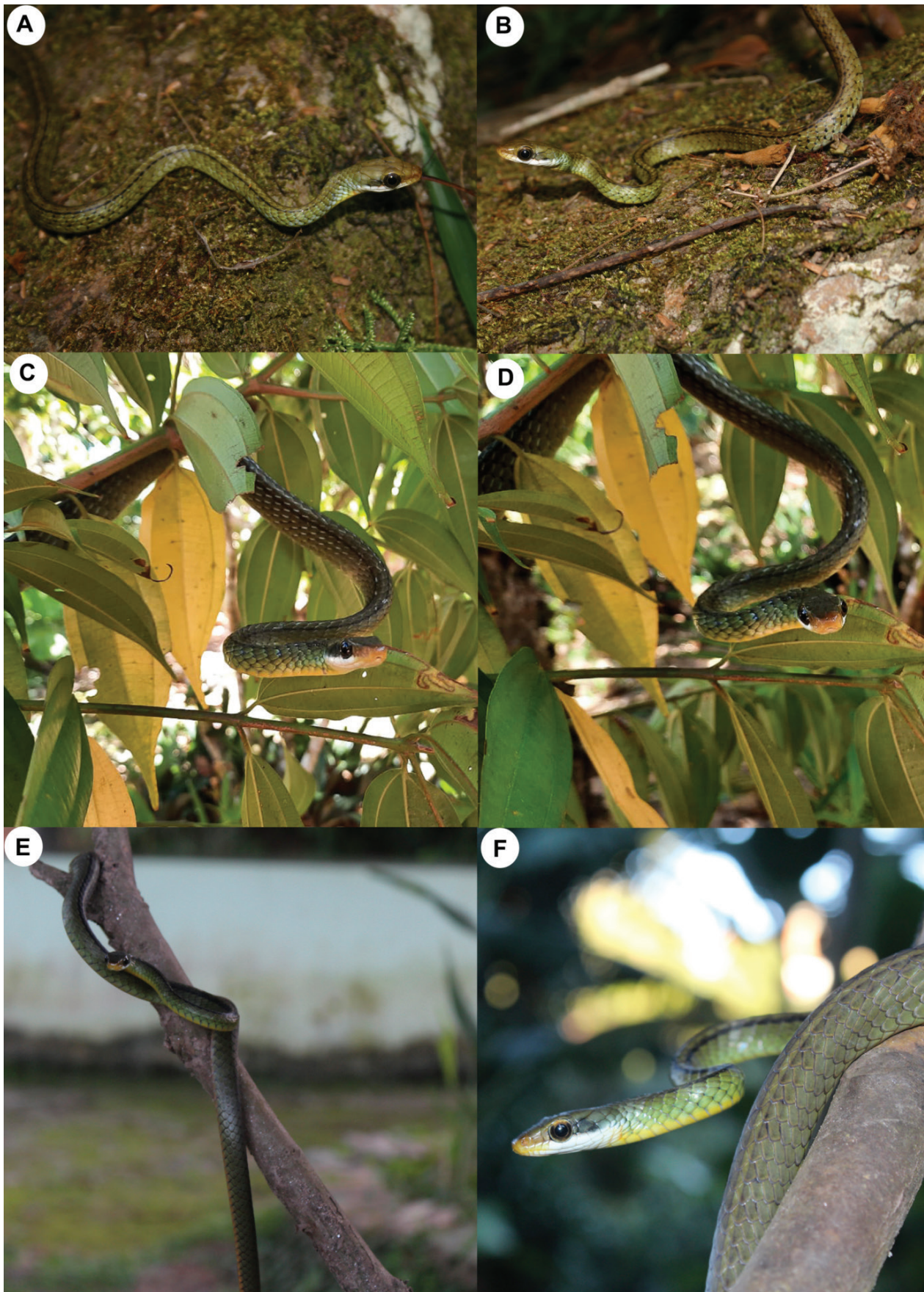


Figure 12. General view while alive of *Chironius dracomaris* sp. nov.: **A, B** a specimen (IBSP 76994 or 76995) from Sítio Álvaro, municipality of Guaramiranga, state of Ceará, Brazil. These two vouchers were destroyed in a fire on May 15, 2010, leaving only photographic records of one of the specimens while alive; **C–F** paratypes of *Chironius dracomaris* sp. nov. (MNRJ 27803 and MHNCE-R 577, respectively) from Museu de História Natural do Ceará Prof. Dias da Rocha, municipality of Pacoti, state of Ceará, Brazil. Photos by I.J. Roberto (A, B), R.C. Gonzalez (C, D), T. Cavalcante (E, F).

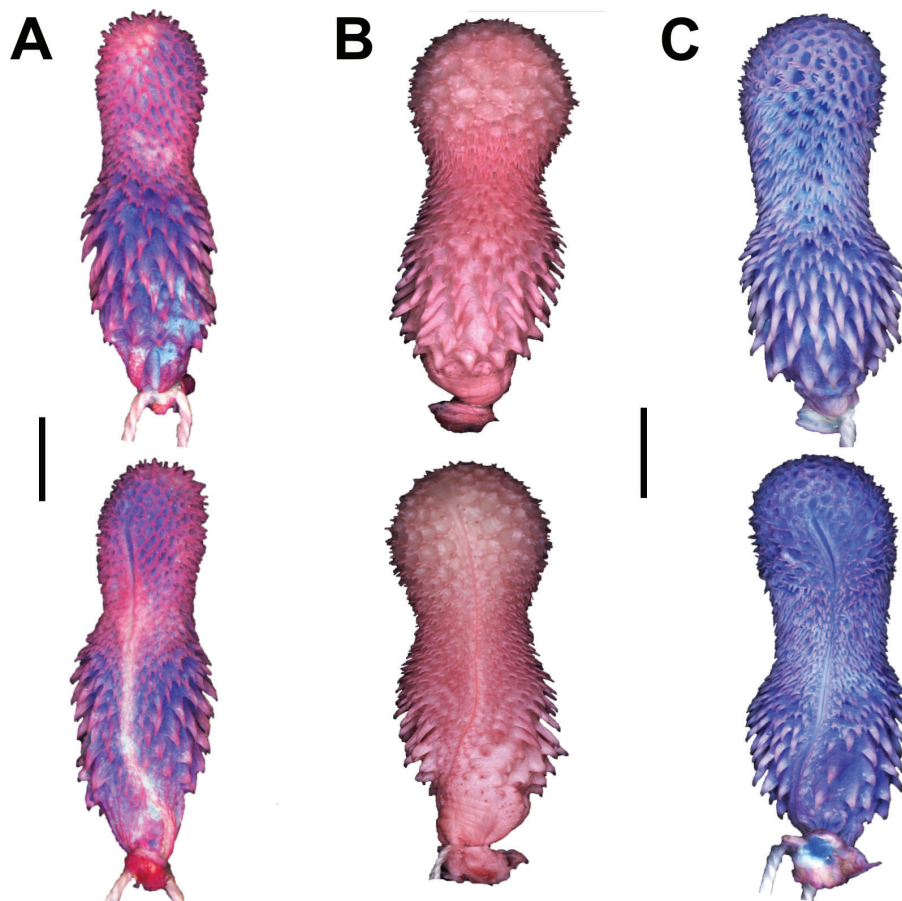


Figure 13. Asulcate (above) and sulcate (below) views of the hemipenis of: **A** the holotype of *Chironius dracomaris* **sp. nov.** (MNRJ 27716) from Horto Florestal, Granja neighborhood, municipality of Pacoti, state of Ceará, Brazil; **B** *Chironius bicarinatus* (MNRJ 25558) from the municipality of Petrópolis, state of Rio de Janeiro, Brazil; **C** *Chironius gouveai* (MHNCI 12369) from the municipality of Candói, state of Paraná, Brazil. Scale bar = 5 mm.

Braincase. Prefrontals: in contact with frontals dorsally, and approaching the maxillary process of palatine making little contact on only one side ventrally; in anterodorsal view, they present a process directed medially in basal portion; in lateral view, lacrimal foramen visible in basal portion; broad and rounded anterior process; posterior portion concave, forming anterior border of orbital cavity; large lacrimal foramen without a conspicuous projection on the anteroventral surface; **frontals:** in dorsal view, frontals in contact, with a straight medial suture; anterior margin rounded; anterolateral margins oblique and in contact with prefrontals; posterolateral margins slightly curved, forming the dorsal margin of orbital cavity; suture contacting parietals oblique, with the presence of foramina in the posterolateral region of frontals; vertical laminae in contact with parabasisphenoid ventrally and septomaxilla anteriorly; **parietal:** in dorsal view, almost rounded, as long as broad, with depressions on the mesoanterior and lateral margins, forming ridges on the lateral margins; anterior margins oblique in contact with frontals; also form posterodorsal border of orbital cavity; it contacts postorbital anterolaterally; posterior margins rounded in contact with supraoccipital medially; in lateral and ventral views, contacts posterior portion of parasphenoid rostrum anteriorly and basisphenoid lateromedially; posterolaterally contacting anterior margin of prootics and supratemporals; **postorbitals:** long, slightly curved, forming the posterolateral margin of the orbital cavity; they contact lateral process of parietal dorsomedially, but do not make contact in the

basal region; no contact with frontals and broadly separated from ectopterygoid; **supraoccipital:** in dorsal view, subpentagonal, broader than long, oblique anterior and posterior margins, in contact with parietal anteriorly, with prootics laterally and exoccipitals posteriorly positioned; a constriction in the mesolateral region creates a depression with a foramen in the posterior part; conspicuous medial crests, between these crests emerges a pronounced medial crest perpendicularly in the posterior region, separating two depressions, each one presenting a foramen in basal region; **exoccipitals:** with a medial constriction and continuing lateral ridges; contact supraoccipital anteriorly, prootics and supratemporals laterally, and basioccipital ventrally; in lateral view, form posterior margin of fenestrae ovalis in contact with prootic anteriorly; presence of foramina ventrally and laterally on posterior margin; also forms the dorsal, lateral, and lateroventral margins of the foramen magnum; columella directed to the inner surface of quadrate; **basioccipital:** hexagonal, contacting parabasisphenoid complex anteriorly, prootics and exoccipitals, anterolaterally and posterolaterally, respectively; also forms ventral margin of foramen magnum posteriorly; with two conspicuous medial ridges; a larger perpendicular crest emerges between these ridges that extends to the posterior region; **prootics:** overlain by supratemporals in dorsal region; contacts parietal dorsally and anterolaterally, parabasisphenoid complex and basioccipital ventrally, supraoccipital dorsoposteriorly, and exoccipital posterolaterally; in lateral view, each with two large and three small fo-

ramina (two below the large foramina and one above); posteriorly, form anterior margin of fenestrae ovalis in contact with exoccipitals; **parabasisphenoid complex:** basisphenoid and parasphenoid fused in ventral view, but separate in dorsal view; in dorsal view, basisphenoid trapezoidal shaped, with a large median cavity, and spear shaped parasphenoid, tapering from the level of anterior margin of ectopterygoid, surpassing the palatine choanal process; basisphenoid contacts basioccipital posteriorly, prootic and parietal posterodorsally; parasphenoid contacts frontal dorsoanteriorly, and approaches, but does not contact posterior vomers and choanal process of palatine anteroventrally; in dorsal view, parasphenoid rostrum with lateral groove on each side along its length, with extension on medial part; in ventral view, posterior part of parasphenoid rostrum presents an extension laterally; in ventral view, basisphenoid has two lateral ridges, one extending to suture of prootic and the other to the half where two foramina are present; two further foramina are present on each side of basisphenoid anterior to the ridges.

Palatomaxillary arch. Maxillae: elongated (sensu Klaczko et al. 2014), extends to the level of vomerine premaxilla processes to posterior border of postorbital, surpassing the palatine medially; in dorsal view, arched towards premaxilla in anterior portion, with a constriction at the level of prefrontal, which present a lateral extension approaching palatine; presence of a foramen anteriorly to the lateral extension; posterior portion with a lateral extension with a slight overlap with ectopterygoid, but without contact, forming the inferior margin of orbital cavity; ventral surface with 34–36 subequal, curved, and rear facing teeth, increasing in size towards the last five teeth; **ectopterygoids:** narrow, slightly curved; semicircle-shaped anterior margin with a rectangular lateral process, that overlaps maxilla; slightly curved posterior process; ventral surface of posterior portion in contact with dorsolateral surface of pterygoid medially; **pterygoids:** elongated, corresponding approximately to slightly more than half the size of braincase; ventral surface with 30–31 subequal, curved, and rear facing teeth; anterior portion tapered, presenting a slight overlap with posterior portion of palatine and gradually widening from the region of contact with ectopterygoid in anteroposterior direction, tapering again near the rounded posterior end, where both move away in curvature approaching quadrate-compound bone joint laterally; dorsal surface with a lateral longitudinal ridge from the posterior level of contact with ectopterygoid, extending almost to the end of the broad posterior region; **palatines:** slender, almost straight; ventral surface with 24 subequal, slightly curved, and rear facing teeth; in dorsal view, almost contacting globular portion of vomers in anterior portion; choanal process dorsomedially directed toward parasphenoid rostrum, but without contact; short maxillary process situated at level of anterior border of choanal process on lateral surface of palatine, directed posterolaterally, contacting small portion of prefrontal ventromedial surface, but no contact with

palatine process of maxilla; presence of a foramen in the medial region of maxillary process; a short bifurcation before the pterygoid contact zone in posterior portion, with medial branch longer than lateral branch; the medial branch overlaps and contacts the anterior border of pterygoid.

Suspensorium and mandible. Supratemporals: subrectangular, elongated, slightly curved lateromedially; anterior portion does not surpass parietal–prootic suture; overlapping and contacting prootic and exoccipital laterally, with half of supratemporal articulating with quadrate laterally; posterior end straight, surpassing the posterior portion of exoccipital; **quadrates:** flattened and broad dorsally, tapering and slightly curving dorsoventrally; dorsal portion contacting supratemporal laterally; medial portion with short process, near columella auris; ventral portion articulates with compound bone; ventromedial portion approaching, but not in contact with pterygoid; **dentaries:** medially curved anteriorly; dorsal surface with 35–36 subequal, slightly curved, rear facing teeth, decreasing in size posteriorly; lateral face convex with a mental foramen medially on one side and ventrally on the other; posterior to this foramen, a bifurcation of dorsal and ventral processes laid over the compound bones in anterior part, with dorsal process longer than ventral; again, dorsal process bifurcates a short medial process, with presence of dentition only in the longer process; ventral process contacts splenial and angular, in addition to compound bone; Meckelian fossa is delimited by the dentary and splenial; **splenials:** elongated, tapered anteriorly, in the region of contact with dentary; posterior part in contact with anterior region of angular; anterior mylohyoid foramen situated below dorsal extension; **angulars:** elongated, tapered posteriorly, contacting compound bone laterally, and dentary and splenial anteroventrally; posterior mylohyoid foramen near suture with splenial; in ventral view, angular-splenial joint visible on one side; **compound bones:** elongated, approximately two-thirds length of mandible; in lateral view, tapers anteriorly; in contact with dentary posteriorly; presence of a foramen laterally to the posterior tip of angular; prearticular crest prominent, distinctly higher than surangular crest; a rounded depression where it articulates with the quadrate; retroarticular process medially directed.

Meristic and morphometric variation. The largest specimen was a male CHUFC 2626 (TL = 991 mm, SVL = 639 mm, CL = 352 mm); the largest female was CHUFC 3305 (TL = 951 mm, SVL = 604 mm, CL = 347 mm); tail 50–57% SVL (53 ± 2 , 13) in females, 54–56% SVL (55 ± 0.7 , 6) in males; ventrals 154–162 ($156.7 [155.9, 157.4] \pm 2.2$, 34) in females, 149–159 ($153.6 [152.9, 154.7] \pm 2.1$, 27) in males; subcaudals 124–135 ($129.3 [127.7, 130.9] \pm 2.7$, 13) in females, 132–138 ($133.6 [131.3, 136.0] \pm 2.2$, 6) in males; cloacal plate divided and 12/12/10 dorsal scale rows in both sexes ($n = 59$, 100% of the sample); two postoculars ($n = 53$, 91%; one postocular: $n = 3$, asymmetric variants with 1/2 postoculars: $n = 2$);

nine supralabials (n = 52, 88%; eight supralabials: n = 3, asymmetric variants with supralabials 9/8 or 10/9: n = 4); infralabials 10 (n = 34, 59%; infralabials 9: n = 5, infralabials 11: n = 2; asymmetric variants with infralabials 9/10 or 11/10: n = 17, 29%). Additional meristic and morphometric variation of characters for *Chironius dracomaris* are in Table 1.

Etymology. The specific epithet *dracomaris* is the conjunction of two nouns “*draco*” (nominative) and “*maris*” (genitive), used in apposition with the Latinized nickname “Dragão do Mar” (= Dragon of the Sea, in English), as Francisco José do Nascimento (1839–1914) became historically known. He was a popular leader of the harbor pilots in Ceará, who became a symbol of Northeastern resistance against slavery in Brazil. In 1881, “Dragão do Mar” led one of the main port stoppage movements, refusing to transport slaves to the ships, thus preventing interprovincial trafficking. The successive closures of the port accelerated abolitionism in the region, which made Ceará the first Brazilian province to banish slavery, on March 25, 1884, four years before the signing of the Lei Aurea (Morel 1967). The recent worldwide manifestations (Black Lives Matter movement) are proof that we need to change and repair social and historical injustices (see Subbaraman 2020). The fight against modern slavery and structural racism still permeates in Brazil. For example, in the city where “Dragão do Mar” was born (Aracati, Ceará), there are social-environmental conflicts over the traditional use of the territory, as well as in several other areas (Nascimento 2018; Quilombola community of Cumbe). In 2019, the winning Samba of Rio de Janeiro’s Carnival—História Para Ninar Gente Grande from the school Estação Primeira de Mangueira—honored “Dragão do Mar”, as well as other symbols of black and peripheral resistance against exploitation in Brazil, for example the councilor Marielle Franco, who was brutally murdered by the Rio de Janeiro militia on March 14, 2018. We dedicate this species to Francisco José do Nascimento “Dragão do Mar” and these leaders who inspire the daily struggle of restoring a democratic environment in Brazil.

Distribution (Fig. 8). Based on the current evidence, *Chironius dracomaris* is restricted to the “Brejo de altitude” from Baturité Massif (known records in the municipalities of Baturité, Guaramiranga, and Pacoti), enclaves of remaining rainforests in the dry Caatinga domain of northeastern Brazil, state of Ceará, between 500–800 m a.s.l..

Remarks. Loebmann and Haddad (2010) recorded a specimen tentatively identified as *Chironius bicarinatus* (IBSP 77076) from the Ibiapaba Plateau, the westernmost rainforest fragments of the “Brejo de Altitude” in the state of Ceará. Unfortunately, the voucher was destroyed in a fire on May 15, 2010 (Franco 2012), and it was therefore, not possible to check the accuracy of its identification and thus confirm the occurrence of *C. dracomaris* also in the Ibiapaba Plateau.

Discussion

The main taxonomic reviews that have addressed the name *Chironius bicarinatus* (Bailey 1955; Dixon et al. 1993), used composite sampling that included specimens, later described by Entiauspe-Neto et al. (2020), as *C. gouveai*. Nonetheless, even Dixon et al. (1993) suspected that the southern populations could represent a new taxon, presenting differences in color pattern, the sum of segmental counts, number of maxillary teeth, frequency of temporals 1+1, and the occurrence into a distinct phytophysiognomy. All these morphological features and ecological preferences were corroborated in the present study, in addition to molecular evidence of a distinct lineage herein described and named as *C. dracomaris* **sp. nov.** (Figs 1–5). *Chironius dracomaris* **sp. nov.** is distinguished from *C. bicarinatus* and *C. gouveai* by the combination of qualitative and quantitative morphological characters (general body coloration, meristic, body proportion, frequency of temporals and apical pits along the body, and cranial osteology with respect to *C. gouveai*). Table 5 shows comparisons of the most frequent qualitative and osteological characters among the species.

Some information (diagnosis, geographical distribution, and material examined) present in the original description of *Chironius gouveai* (Entiauspe-Neto et al. 2020) should be considered with caution. The frequency of many characters mentioned in the topics of “emended diagnosis” and “description” for *C. bicarinatus* and “definition and diagnosis” for *C. gouveai* differ from our own results (Table 6). In addition, most of the characters used by Entiauspe-Neto et al. (2020) in the comparisons between *C. gouveai* and *C. bicarinatus* did not have their polymorphism levels tested properly with dense geographic sampling. They distinguish *C. gouveai* from *C. bicarinatus* (in parentheses) based on the following characteristics: “white gular coloration in life (vs. yellow), reticulated dorsal pattern in adults (vs. uniform green), dorsal pattern with scattered black blotches in juveniles (vs. black transversal bars), absent or vestigial postocular stripe (vs. present on adults and juveniles, rarely vestigial on juveniles), hemipenis smooth calyculate apex (vs. spinulate calyces)” (Entiauspe-Neto et al. 2020). These features observed from specimens while alive did not have the polymorphism levels tested due to the small sample size, while hemipenial morphology characters are polymorphic in our sample, and are not fixed in any populations of either species. With respect to the osteological characters used in the comparisons by Entiauspe-Neto et al. (2020), three characters (presence of a conspicuous projection on the ventral surface of the septomaxilla; presence of a conspicuous projection on anteroventral surface of prefrontal lacrimal foramen; and posterior portion of supratemporals slightly curved) seem to be fixed for *C. gouveai*, while the character anterior portion of the supratemporal bones surpassing the parietal–prootic suture is polymorphic in our sample. Despite the small sample size, we found an additional difference related to the number of palatine teeth (23–24 teeth in *C. bicarinatus* vs. 16–18 in *C. gouveai*).

Table 5. Comparisons of the most frequent diagnostic characters (qualitative, osteological) among *Chironius bicarinatus*, *C. gouveai* and *C. dracomaris sp. nov.*

Characters	<i>C. bicarinatus</i>	<i>C. gouveai</i>	<i>C. dracomaris sp. nov.</i>
Dorsal color pattern	Uniformly green, olive or grayish olive dorsum	Uniformly light brown, grayish olive or olive dorsum with black or brown edge in the scales	Uniform green or olive dorsum with two black dorsolateral stripes
Belly color pattern	The first third of the belly and subcaudals yellowish; the remainder of the belly whitish yellow	The first third of the belly (can also be whitish) and subcaudals yellowish or brownish yellow; the remainder of the belly whitish yellow or brownish yellow; ventrals with black or brown edges	The first third of the belly, near cloacal region and subcaudals whitish; the remainder of the belly olive or greenish
Subcaudals color pattern	A medially positioned black zig-zag line between subcaudals, gradually fading to the tip of the tail; outer margins with a black outline	Subcaudals with black or brown edges; outer margins with a black outline	Subcaudals with slightly black edges; outer margins without a black outline or a black zig-zag line medially positioned between subcaudals
Temporals	Usually 1+2	Usually 1+1	Usually 1+2
Apical pits	Usually only on the neck region of the body	Only on the neck region of the body	On the neck and in at least one other region of the body
Conspicuous projection on ventral surface of the septomaxilla	Absent	Present	Absent
Conspicuous projection on anteroventral surface of prefrontal lacrimal foramen	Absent	Present	Absent
Quadrato-suspensorium articulation with posterior end of supratemporals	Straight	Slightly curved	Straight

Table 6. Comparisons between character frequencies and specimen identifications in the sample examined by Entiauspe-Neto et al. 2020 with the results of this study.

Character frequencies	Entiauspe-Neto et al. 2020 (n = 79)	This study (n = 434)
	<i>Chironius bicarinatus</i>	
Temporals	1+1 (79%)	1+2 (66%; n = 167)
Supralabials	eight (61%)	nine (92%; n = 174)
Infralabials	eight (72%)	ten (73%; n = 136)
Dorsal scale rows	12/12/10 (56%)	12/12/10 (100%; n = 229)
	<i>Chironius gouveai</i>	
Subcaudal range in females	103–146	139–146 (n = 10)
Infralabials	eight (74.2%)	ten (71%; n = 98)
Specimen identifications		
CHUFC 1389, 2103, 2597, 3249, 3300	<i>Chironius bicarinatus</i>	<i>Chironius dracomaris sp. nov.</i>
IBSP 10908, 21568, 64234	<i>Chironius bicarinatus</i>	Vouchers destroyed in a fire accident that hit the Instituto Butantan on May 15, 2010. Probably not be specimens of <i>C. bicarinatus</i> , as there is no additional voucher for Mato Grosso do Sul State.
MCP 4134, 4283, 4199, 4244, 17291, MHNCI 1662, 5328, 8428, 10502	<i>Chironius bicarinatus</i>	<i>Chironius gouveai</i>
MZUFV 45, 145, 168, 642	<i>Chironius bicarinatus</i>	<i>Chironius quadricarinatus</i> Boie, 1827
UFMG 86 (field number: 1610)	<i>Chironius bicarinatus</i>	<i>Chironius brazilii</i> Hamdan & Fernandes, 2015
UFPB 77	<i>Chironius bicarinatus</i>	<i>Leptophis dibernardoi</i> Albuquerque, Santos, Borges-Nojosa & Ávila, 2022
MCP 312, 1711, 3724, 15530	<i>Chironius foveatus</i>	<i>Chironius gouveai</i>
MHNCI 12369, MCP 2423	<i>Chironius cf. exoletus</i>	<i>Chironius gouveai</i>

Regarding the geographical distribution presented by Entiauspe-Neto et al. (2020), the authors mention that *Chironius bicarinatus* and *C. gouveai* are allopatric, but

they present a distribution map (Entiauspe-Neto et al. 2020: fig. 2) with examined specimens (circles) and literature records (squares), where the species are clearly

parapatric, presenting sympatry in several localities. This distribution map differs greatly from the one herein presented (Fig. 8), which was constructed based solely on records of specimens that were examined first-hand, except for ten additional specimens that were examined through photographs (Appendix 1). Although both species present distribution borders that are close to one another, their niche overlap is low, which indicates that niche divergence may be involved in the evolution of the group (Fig. 8, Table 4; see Wiens and Graham 2005). We examined 46 specimens included in the list of material examined by Entiauspe-Neto et al. (2020), of which 23 (50%) were redetermined (Table 6). From the geographic distribution (western Paraná State), we estimate that another 39 specimens identified as *C. bicarinatus* by Entiauspe-Neto et al. (2020), which we were not able to examine, may actually be *C. gouveai*. Therefore, we disagree with these identifications given by Entiauspe-Neto et al. (2020) and we believe that they did not examine the number of specimens mentioned, which is clearly perceptible based on the number of specimens used in the comparative table of variation between *C. gouveai* and *C. bicarinatus* (“table 1”, $n = 79$), when compared to the list of specimens examined (“Materials and Methods” and “Appendix II – Specimens examined”, $n = 279$). Thus, it seems as though the description of *C. gouveai* was broadly based on photographs and unreliable information in the literature that was cited as examined material and used for comparisons. Therefore, we emphasize the importance of taxonomic efforts with denser sampling and the verification of the literature records (Willis 2003; Passos et al. 2022). The power of a species’ diagnostic characters, delimitation boundaries with its closest related species and the knowledge of its geographical distribution, are more useful than species descriptions, which must be the main aim in taxonomic studies.

Many endemic reptile and amphibian species have been described in the “Brejos de Altitude” (i.e., isolated remnants of rainforest restricted to highlands throughout the xerophytic Caatinga domain), mostly from the Baturité Massif in Ceará State (e.g., Hoogmoed et al. 1994 for *Adelophryne baturitensis* and *A. maranguapensis*; Passos et al. 2007 for *Atractus ronnie*; Roberto et al. 2014 for *Rhinella casconi*; Borges-Nojosa et al. 2016 for *Placosoma limaverdorum*; Mângia et al. 2018 for *Proceratophrys ararype*; and, Roberto et al. 2022 for *Pristimantis relictus*). In fact, there is already a report in the literature of a possible new species of the genus *Chironius* occurring in a “Brejo de Altitude”. Hamdan et al. (2017) highlighted the populations currently assigned to *C. flavolineatus* from Serra da Ibiapaba, state of Ceará, as a candidate species inferred from a coalescent-based phylogeny covering the entire genus. Thus, further investigations are being made by Hamdan et al. (2017) for the formal recognition (or not) of this lineage. The biota inhabiting these relictual forests in northeastern Brazil is also a result of historical connections between enclaves and the Amazon and/or Atlantic rainforests, with endemic species serving as witnesses of speciation events which occurred as a result of the geographical isolation of these enclaves across the

Caatinga (Vanzolini 1981; Coimbra-Filho and Câmara 1996). Currently, the spatial or temporal scales of these historical connections are under debate and new evidence suggests complex evolutionary histories involving multiple events and processes triggering high-level endemism found in these relictual forests (Batalha-Filho et al. 2013; Peres et al. 2020).

Furthermore, the São Francisco River seems to act as a physical barrier (Carnaval and Moritz 2008; Recoder and Rodrigues 2020; Thomé et al. 2021) to gene flow in some disparate taxa, such as lizards, amphisbaenians and snakes (Rodrigues 1996; Passoni et al. 2008; Bruschi et al. 2019). In fact, the São Francisco River apparently limits the northern distribution of *C. bicarinatus* and separates it from the area of occurrence of *Chironius dracomaris* **sp. nov.** for more than 800 km of airline. Rodrigues (1996) proposed the Paleolacustrine Vicariance Hypothesis in order to explain the recovered pattern of some lizards as sister-species on the opposite sides of the banks of the São Francisco River. This hypothesis is in accordance with estimates of divergence times among species on opposite banks of the river (Recoder and Rodrigues 2020).

The molecular phylogeny recovered *Chironius dracomaris* **sp. nov.** as a sister-group of the clade *C. bicarinatus* + *C. gouveai* (Fig. 1), which could suggest the existence of a connection between the “Brejos de Altitude” and Atlantic Forest, with the São Francisco River acting as a secondary barrier. However, additional phylogeographic and paleoclimatic studies are necessary to understand the evolutionary history of these lineages. The projection models for *C. bicarinatus* suggest that the connectivity of the suitable areas in the Atlantic Forest with the Baturité Massif, where *C. dracomaris* **sp. nov.** occurs, may be older than the Last Interglacial (120 kyr) (Fig. 5), as proposed by Silveira et al. (2019) with woody plant species. On the other hand, the southern limit of the distribution of *C. bicarinatus* in Serra do Tabuleiro, state of Santa Catarina, is very close to the area of occurrence of *C. gouveai*, being separated by Serra do Mar, with *C. bicarinatus* occurring along the coast in Ombrophilous Dense Forests and *C. gouveai* occurring in inland Serra do Mar at higher altitudes in Mixed and Semideciduous Forests (Fig. 8). Coincidentally, Serra do Tabuleiro also appears to be the southern limit of the other Atlantic species of the genus (*C. foveatus*, *C. fuscus*, and *C. laevicollis*), except for *Chironius* cf. *exoletus*, which extends its distribution to the region of Porto Alegre, state of Rio Grande do Sul, already in a transition area with the Pampas. Despite the low genetic distances between *C. gouveai* and *C. bicarinatus* (0.4–3.7%; Table S1), we recognize both as valid species because they were recovered as reciprocal monophyletic taxa (Fig. 1). In addition, both species are fully diagnosable on the basis of phenotypic characters with low niche overlap, and ultimately, we do not establish cut-off for genetic distances as a criterion for species delimitation due to gaps in geographic sampling (see Fig. 8B, C). As *C. bicarinatus* and *C. gouveai* are broadly distributed across Tropical Atlantic and Subtropical climates, respectively, the bioclimatic variables that were most related are characterized by these climates,

with the Tropical Atlantic presenting higher temperatures with precipitation concentrated in winter, and the Sub-tropical presenting milder and more well-distributed precipitation throughout the year (Tables S3, S5).

We believe that the continental shelf in the LGM, an area currently submerged along the Brazilian coastline, possibly during periods of climatic oscillations and marine regressions (see Leite et al. 2016), could have sheltered an extensive and suitable area for the *Chironius bicarinatus* lineage. This hypothesis perhaps made it possible for ancestral populations to expand their distribution vertically to the northern limits of the Atlantic Forest. The projection models support the expansion of suitable areas in the LGM with the distention of the continental shelf, suggesting that previous Holocene events may have favored a bottleneck effect related to the consolidation of the speciation process previously initiated between *C. bicarinatus* and *C. gouveai*. On the other hand, although some coastal populations may have speciated prior to the LGM, other snake species likely diverged within the last 11,000 years (see Barbo et al. 2022). In this scenario, sea-level transgressions along the coastline (see Castro et al. 2014), may have triggered the interruption of the Atlantic Forest lowland corridor in the case of *Chironius bicarinatus* dispersion due to the close proximity between the Serra do Mar Mountain range and the Atlantic Ocean. In addition, the Paranapanema River (concordant with the neotectonic barrier of the Guapiara lineament), also appears to act as a potential barrier, limiting the northern distribution of *C. gouveai*, which is also observed in other taxa (e.g., Graziotin et al. 2006 with the snakes of the *Bothrops jararaca* complex; Brunes et al. 2010 with the treefrogs of the *Phyllomedusa burmeisteri* group). Reinforcing this hypothesis, we noted that populations of *Chironius gouveai* near Serra do Mar, in the states of Paraná and Santa Catarina, have a color pattern that is more similar to *C. bicarinatus* than those that occur further inland. We encourage further research on the existence of putative hybrids in this contact zone in Serra do Mar, introducing the possibility of evaluating the effective barriers that currently act on the southern limits between the species. For instance, our data reinforce the need to complement the conservation policy proposed by Álvarez-Presas et al. (2014), which suggested extending the southern limit of the Serra do Mar corridor to embrace the Parque Nacional da Serra do Itajaí and Parque Estadual da Serra do Tabuleiro, as these areas are also part of a relevant biogeographical province in the Serra do Mar Mountain range (Klein 1981; Álvarez-Presas et al. 2014).

Similarly, it would also be extremely important to conserve the areas of “Brejos de Altitude” (Tabarelli and Silva 2003) and essential to elucidate the evolutionary history of the Atlantic Forest and the diversification processes of its biota. To achieve this, more research is needed in the “Brejos de Altitude” to understand the real richness of the biota and develop conservation and political strategies to conserve threatened species, such as *Chironius dracomaris* **sp. nov.** whose distribution is restricted to Baturité Massif. Nowadays it is widely acknowledged that the Baturité Massif region is suffering from considerable

impacts related to urban expansion, extractive production, agriculture, and cattle ranching, which contribute to forest fragmentation and habitat loss (Coimbra-Filho and Câmara 1996; Borges-Nojosa 2007). Through the newly described species, *Chironius dracomaris* **sp. nov.**, we are hopeful for a change in social and political awareness in relation to the importance of racial equality and the conservation of crucial areas for understanding biodiversity.

Acknowledgments

We are indebted to all curators, technicians and researchers for allowing access to specimens under their care and the assistance received during the visits to their respective institutions, as well as helping to provide specimen data and loans requested: S. Bogan (CFA), D.M. Borges-Nojosa, C.H. Bezerra (CHUFC), B.M. Sousa, R.H. Carvalho (CHUFJF), D. Matos, R.G. Faria (CHUFS), S. Neckel-Oliveira, S.D. Weiermann-Oliveira (CHUFSC), D.O. Mesquita, F.R. Delfim (CHUFPPB), G. Colli, P.P.U. Aquino (CHUNB), S. Kretzschmar (FML), F.C. Resende, G.A. Cotta (FUNED), F.G. Graziotin, F.L. Franco, L.M. Correa, V.J. Germano (IBSP), M.T. Rodrigues (IB/USP), J. Faivovich, S.J. Nenda (MACN), D.J. Santana, P.S. Carvalho (MAP), H.Q.B. Fernandes, J.P. Silva (MBML, INMA/MCTI); R.B. Oliveira (MCN), L.B. Nascimento (MCNR), J. Romanzini, S. Castroviejo-Fisher (MCP), F.B. Dias, C. Ma, R.M. Lira-da-Silva (MHNBA), J.C. de Moura-Leite (MHNCT), D.C. Lima, E.W.P. Santana, R.C. Gonzalez (MHNCE-R), D. Arrieta (MNHN), M. Voitovicz-Cardoso, P.H. Pinna (MNRJ), A.L.C. Prudente, A.C. Ascenso, J.F.M. Sarmiento (MPEG), I. Biondi (MZFS), H. Frossard, O.A. Shibatta (MZUEL), J.A. de Jesus, T.T. Medeiros, A.J.S. Argôlo (MZUESC), J.J.M. Guedes, R.N. Feio (MZUFV), A.B. Carvalho, A.S. Benetti, A.L.M. Braga, F.A.B. Silva, H. Zaher (MZUSP), D. Marques, U. Wüest (NMB), P.C.A. Garcia, H.C. Costa (UFMG), M.R.S. Pires, P.S. Barbosa (UFOP), M. Borges-Martins, G.M.F. Pontes (UFRGS), K. Rebelo, P.R. Manzani (ZUEC), G. Gracioli, T.R.F. Sinani (ZUFMS), D.S. Fernandes (ZUFRJ) E. Elgue, M. Meneghel (ZVC). We thank A.S. Machado, R.T. Lopes (COPPE/UFRJ) for images of scanned skulls. We are indebted to J.C. Ferreira-Junior for help with μ CT images, J. Faivovich for provide the sequences of a *Chironius gouveai* specimen. S. Marques-Souza, M. Borges-Martins, J.A. Oliveira, M. Bilate, F. Dias-Silva, O.L. Balbinot, I.J. Roberto, R.C. Gonzalez, T. Cavalcante for kindly provide photographs of species while alive. O.R. Padilla, A.L.G. Carvalho for providing photographs of some specimens from MCP and ZUEC collections, respectively. L. Ugioni, S.J. Nenda contributed to important discussions in previous versions of the manuscript. D.S. Fernandes, B. Hamdan and two anonymous reviewers provided constructive criticisms that considerably improved early versions of the manuscript. R.C. Gonzalez, M.A. Crozariol, A.C. de Araújo provided invaluable help in obtaining data from specimens of populations in the Baturité Massif. G.A. Elias for the help during the searches for botanical references. We are grateful for the sequencing services provided by Centro de Estudos do Genoma Humano e Células-Tronco from Universidade de São Paulo and Rede de Plataformas Tecnológicas da Fundação Oswaldo Cruz. V.S. and A.A. Jr. Thank the Coordenação de Aperfeiçoamento de Pessoal de Nível Superior (CAPES) for the doctoral scholarships (processes 88887.201311/2018-00 and 88887.371704/2019-00, respectively). The other co-authors were financial support by the following research fellowships: J.A.R.A. Conselho Nacional de Desenvolvimento Científico e Tecnológico (CNPq) (#300739/2022/2); R.W.A. CNPq (#305988/2018-2; 307722/2021-

0) and FUNCAP (process UNI-0210-00556.01.00/23); F.F.C. CNPq (#449898/2014-3); P.M.S.N. CNPq (#313622/2018-3; 309253/2021-7); PP. CNPq (#307631/2021-4) and Fundação Carlos Chagas Filho de Amparo à Pesquisa do Estado do Rio de Janeiro (#E-26/202.737/2018).

References

- Achaval F, Gonzalez JG, Meneghel DM, Melgarejo AR (1979) Lista comentada del material recogido en costas uruguayas, transportado por camalotes desde el Río Paraná. *Acta Zoologica Lilloana* 35: 195–200.
- Adobe Inc (2019) Adobe Photoshop. Available from: <https://www.adobe.com/products/photoshop.html>
- Aiello-Lammens ME, Boria RA, Radosavljevic A, Vilela B, Anderson RP (2015) spThin: An R package for spatial thinning of species occurrence records for use in ecological niche models. *Ecography* 38: 541–545. <https://doi.org/10.1111/ecog.01132>
- Akaike H (1974) A new look at the statistical model identification. *IEEE Transactions on Automatic Control* 19: 716–723. <https://doi.org/10.1109/TAC.1974.1100705>
- Altschul SF, Madden TL, Schäffer AA, Zhang J, Zhang Z, Miller W, Lipman DJ (1997) Gapped BLAST and PSI-BLAST: A new generation of protein database search programs. *Nucleic Acids Research* 25: 3389–3402. <https://doi.org/10.1093/nar/25.17.3389>
- Álvarez-Presas M, Sánchez-Gracia A, Carbayo F, Rozas J, Riutort M (2014) Insights into the origin and distribution of biodiversity in the Brazilian Atlantic Forest hot spot: A statistical phylogeographic study using a low-dispersal organism. *Heredity* 112: 656–665. <https://doi.org/10.1038/hdy.2014.3>
- Amaral A (1925) South American snakes in the collection of the United States National Museum. *Proceedings of the United States National Museum* 67: 1–30. <https://doi.org/10.5479/si.00963801.2596>
- Arévalo E, Davis SK, Sites Jr JW (1994) Mitochondrial DNA sequence divergence and phylogenetic relationships among eight chromosome races of the *Sceloporus grammicus* complex (Phrynosomatidae) in Central Mexico. *Systematic Biology* 43: 387–418. <https://doi.org/10.1093/sysbio/43.3.387>
- Bailey JR (1955) The snakes of the genus *Chironius* in Southeastern South America. *Occasional Papers of the Museum of Zoology, University of Michigan* 571: 1–21.
- Barbo FE, Booker WW, Duarte MR, Chaluppe B, Portes-Junior JA, Franco FL, Graziotin FG (2022) Speciation process on Brazilian continental islands, with the description of a new insular lancehead of the genus *Bothrops* (Serpentes, Viperidae). *Systematics and Biodiversity* 20: 2017059. <https://doi.org/10.1080/14772000.2021.2017059>
- Batalha-Filho H, Fjeldså J, Fabre PH, Miyaki CY (2013) Connections between the Atlantic and the Amazonian forest avifaunas represent distinct historical events. *Journal of Ornithology* 154: 41–50. <https://doi.org/10.1007/s10336-012-0866-7>
- Boettger O (1898) *Katalog der Reptilien-Sammlung im Museum der Senckenbergischen Naturforschenden Gesellschaft in Frankfurt am Main. II. Teil (Schlangen)*. Druck von Gebrüder Knauer, Frankfurt am Main, ix + 160 pp.
- Boie F (1826) Notice sur l'Erpétologie de l'île de Java. In: Schlegel H (Ed.) *Ouvrage manuscrit*. *Bulletin des Sciences Naturelles et de Géologie* 9: 233–240.
- Borges-Nojosa DM (2007) Diversidade de Anfíbios e Répteis da Serra de Baturité, Ceará. In: Oliveira TS, Araújo FS (Eds) *Diversidade e conservação da biota na Serra de Baturité, Ceará*. Editora UFC, Fortaleza, 225–247.
- Borges-Nojosa DM, Caramaschi U, Rodrigues MT (2016) A new species of lizard *Placosoma* Tschudi, 1847 (Squamata: Gymnophthalmidae) from the relictual forest mountains of the State of Ceará, Brazil. *Zootaxa* 4169: 160–170. <https://doi.org/10.11646/zootaxa.4169.1.8>
- Boulenger GA (1894) *Catalogue of the snakes in the British Museum (Natural History)*. Volume II. Containing the conclusion of the *Colubridae aglyphe*. Trustees of the British Museum (Natural History), London, xi + 382 pp. + 20 plates.
- Broennimann O, Fitzpatrick MC, Pearman PB, Petitpierre B, Pellissier L, Yoccoz NG, Thuiller W, Fortin MJ, Randin C, Zimmermann NE, Graham CH, Guisan A (2012) Measuring ecological niche overlap from occurrence and spatial environmental data. *Global Ecology and Biogeography* 21: 481–497. <https://doi.org/10.1111/j.1466-8238.2011.00698.x>
- Broennimann O, Di Cola V, Guisan A (2023) *ecospat: Spatial ecology miscellaneous methods*. R package version 3.5. Available at: <https://CRAN.R-project.org/package=ecospat>.
- Brown JL, Hill DJ, Dolan AM, Carnaval AC, Haywood AM (2018) PaleoClim, high spatial resolution paleoclimate surfaces for global land areas. *Scientific Data* 5: 180254. <https://doi.org/10.1038/sdata.2018.254>
- Brunes TO, Sequeira F, Haddad CFB, Alexandrino J (2010) Gene and species trees of a Neotropical group of treefrogs: Genetic diversification in the Brazilian Atlantic Forest and the origin of a polyploid species. *Molecular Phylogenetics and Evolution* 57: 1120–1133. <https://doi.org/10.1016/j.ympev.2010.08.026>
- Bruschi DP, Peres EA, Lourenço LB, Bartoletti LFM, Sobral-Souza T, Recco-Pimentel SM (2019) Signature of the paleo-course changes in the São Francisco River as source of genetic structure in Neotropical *Pithecopus nordestinus* (Phyllomedusinae, Anura) treefrog. *Frontiers in Genetics* 10: 728. <https://doi.org/10.3389/fgene.2019.00728>
- Carnaval AC, Moritz C (2008) Historical climate modelling predicts patterns of current biodiversity in the Brazilian Atlantic Forest. *Journal of Biogeography* 35: 1187–1201. <https://doi.org/10.1111/j.1365-2699.2007.01870.x>
- Carreira S, Meneghel M, Achaval F (2005) *Reptiles de Uruguay*. Universidad de la República, Facultad de Ciencias, Montevideo, 639 pp.
- Carreira S, Maneyro R (2013) *Guía de reptiles del Uruguay*. Ediciones de la Fuga, Montevideo, 285 pp.
- Castro JWA, Suguio K, Seoane JCS, Cunha AM, Dias FF (2014) Sea-level fluctuations and coastal evolution in the state of Rio de Janeiro, southeastern Brazil. *Anais da Academia Brasileira de Ciências* 86: 671–683. <https://doi.org/10.1590/0001-3765201420140007>
- Cei JM (1993) *Reptiles del noroeste, nordeste y este de Argentina*. Herpetofauna de las Selvas Subtropicales, Puna y Pampas. Monografía XIV. Museo Regionale di Scienze Naturali, Torino, 949 pp.
- Coimbra-Filho AF, Câmara IG (1996) Os limites originais do bioma Mata Atlântica na região nordeste do Brasil. *Fundação Brasileira para a Conservação da Natureza, Rio de Janeiro*, 86 pp.
- Cope ED [1860] (1861) *Catalogue of the Colubridae in the Museum of the Academy of Natural Sciences of Philadelphia*. Part. 3. *Proceedings of the Academy of Natural Sciences of Philadelphia* 12: 553–566.
- Cundall D, Irish F (2008) The snake skull. In: Gans C, Gaunt AS, Adler K (Eds) *Biology of the Reptilia*, Vol. 20, Morphology H, The Skull of Lepidosauria. Society for the Study of Amphibians and Reptiles, New York, NY, 349–692.

- De Queiroz K (2007) Species concepts and species delimitation. *Systematic Biology* 56: 879–886. <https://doi.org/10.1080/10635150701701083>
- Di Cola V, Broennimann O, Petitpierre B, Breiner FT, D’Amen M, Randin C, Engler R, Pottier J, Pio D, Dubuis A, Pellissier L, Mateo RG, Hordijk W, Salamin N, Guisan A (2017) ecospat: An R package to support spatial analyses and modeling of species niches and distributions. *Ecography* 40: 774–787. <https://doi.org/10.1111/ecog.02671>
- Dixon JR, Wiest JA, Cei JM (1993) Revision of the Neotropical snake genus *Chironius* Fitzinger (Serpentes, Colubridae). *Museo Regionale di Scienze Naturali* 13: 1–279.
- Dowling HG, Savage JM (1960) A guide to the snake hemipenis: A survey of basic structure and systematic characteristics. *Zoologica* 45: 17–28.
- Duméril AMC (1853) Prodrôme de la classification des reptiles ophiidiens. *Mémoires de l’Académie des Sciences de Paris* 23: 399–536.
- Entiauspe-Neto OM, Lyra ML, Koch C, Quintela FM, Abegg AD, Loebmann D (2020) Taxonomic revision of *Chironius bicarinatus* (Wied 1820) (Serpentes: Colubridae), with description of a new species. *Herpetological Monographs* 34: 98–115. <https://doi.org/10.1655/HERPMONOGRAPHS-D-19-00013.1>
- Farr TG, Kobrick M (2000) Shuttle radar topography mission produces a wealth of data. *Eos* 81: 583–585. <https://doi.org/10.1029/EO-081i048p00583>
- Figueroa A, McKelvy AD, Grismer LL, Bell CD, Lailvaux SP (2016) A species-level phylogeny of extant snakes with description of a new colubrid subfamily and genus. *PLoS ONE* 11: e0161070. <https://doi.org/10.1371/journal.pone.0161070>
- Fitzinger L (1826) Neue Classification der Reptilien nach ihren natürlichen Verwandtschaften nebst einer Verwandtschafts-Tafel und einem Verzeichnisse der Reptilien-Sammlung des K.K. Zoologischen Museum’s zu Wien. J.G. Heubner, Wien, 66 pp. <https://doi.org/10.5962/bhl.title.4683>
- Fitzinger L (1843) *Systema Reptilium. Fasciculus Primus, Amblyglossae*. Braumüller et Seidel, Wien, 106 pp. <https://doi.org/10.5962/bhl.title.4694>
- Franco FL (2012) A Coleção Herpetológica do Instituto Butantan: Da sua origem ao incêndio ocorrido em 15 de maio de 2010. *Herpetologia Brasileira* 1: 22–31.
- Giraud AR (2001) Serpientes de la selva paranaense y del chaco húmedo. *Taxonomía, biogeografía y conservación*. Editorial L.O.L.A., Buenos Aires, 285 pp.
- Grazziotin FG, Monzel M, Echeverrigaray S, Bonatto SL (2006) Phylogeography of the *Bothrops jararaca* complex (Serpentes: Viperidae): Past fragmentation and island colonization in the Brazilian Atlantic Forest. *Molecular Ecology* 15: 3969–3982. <https://doi.org/10.1111/j.1365-294X.2006.03057.x>
- Guedes TB, Nogueira C, Marques OAV (2014) Diversity, natural history, and geographic distribution of snakes in the Caatinga, Northeastern Brazil. *Zootaxa* 3863: 1–93. <https://doi.org/10.11646/zootaxa.3863.1.1>
- Hamdan B, Fernandes DS (2015) Taxonomic revision of *Chironius flavolineatus* (Jan, 1863) with description of a new species (Serpentes: Colubridae). *Zootaxa* 4012: 97–119. <https://doi.org/10.11646/zootaxa.4012.1.5>
- Hamdan B, Pereira AG, Loss-Oliveira L, Rödder D, Schrago CG (2017) Evolutionary analysis of *Chironius* snakes unveils cryptic diversity and provides clues to diversification in the Neotropics. *Molecular Phylogenetics and Evolution* 116: 108–119. <https://doi.org/10.1016/j.ympev.2017.08.004>
- Hammer Ø, Harper DAT, Ryan PD (2001) Past: Paleontological statistics software package for education and data analysis. *Palaeontologia Electronica* 4: 1–9.
- Hijmans RJ, Phillips S, Leathwick J, Elith J (2017) dismo: Species Distribution Modeling. R package version 1.1-4. Cran. Available at: <http://cran.r-project.org/package=dismo>.
- Hijmans RJ (2023) raster: Geographic Data Analysis and Modeling. R package version 3.6-14. Available at: <https://CRAN.R-project.org/package=raster>.
- Hollis JL (2006) Phylogenetics of the genus *Chironius* Fitzinger, 1826 (Serpentes, Colubridae) based on morphology. *Herpetologica* 62: 435–453. [https://doi.org/10.1655/0018-0831\(2006\)62\[435:POTGCF\]2.0.CO;2](https://doi.org/10.1655/0018-0831(2006)62[435:POTGCF]2.0.CO;2)
- Hoogmoed MS, Borges DM, Cascon P (1994) Three new species of the genus *Adelophryne* (Amphibia: Anura: Leptodactylidae) from northeastern Brazil, with remarks on the other species of the genus. *Zoologische Mededelingen* 68: 271–300.
- ICZN [International Commission on Zoological Nomenclature] (1999) International Code of Zoological Nomenclature. The International Trust for Zoological Nomenclature, London, 306 pp. <https://doi.org/10.5962/bhl.title.50608>
- Jan G (1863) *Elenco Sistematico degli Ofidi Descritti e disegnati per l’Iconografia generale*. A. Lombardi, Milano, vii + 143 pp.
- Karger DN, Conrad O, Böhner J, Kawohl T, Kreft H, Soria-Auza RW, Zimmermann NE, Linder HP, Kessler M (2017) Climatologies at high resolution for the earth’s land surface areas. *Scientific Data* 4: 170122. <https://doi.org/10.1038/sdata.2017.122>
- Katoh K, Misawa K, Kuma K, Miyata T (2002) MAFFT: A novel method for rapid multiple sequence alignment based on fast Fourier transform. *Nucleic Acids Research* 30: 3059–3066. <https://doi.org/10.1093/nar/gkf436>
- Klaczko J, Montingelli GG, Zaher H (2014) A combined morphological and molecular phylogeny of the genus *Chironius* Fitzinger, 1826 (Serpentes: Colubridae). *Zoological Journal of the Linnean Society* 171: 656–667. <https://doi.org/10.1111/zoj.12147>
- Klein RM (1981) Fisionomia, importância e recursos da vegetação do Parque Estadual da Serra do Tabuleiro. *Sellowia* 33: 5–54.
- Knight A, Mindell DP (1994) On the phylogenetic relationship of Colubrinae, Elapidae, and Viperidae and the evolution of front-fanged venom systems in snakes. *Copeia* 1994: 1–9. <https://doi.org/10.2307/1446664>
- Kocher TD, Thomas WK, Meyer A, Edwards SV, Pääbo S, Villablanca FX, Wilson AC (1989) Dynamics of mitochondrial DNA evolution in animals: Amplification and sequencing with conserved primers. *Proceedings of the National Academy of Sciences of the United States of America* 86: 6196–6200. <https://doi.org/10.1073/pnas.86.16.6196>
- Kumar S, Stecher G, Li M, Knyaz C, Tamura K (2018) MEGA X: Molecular Evolutionary Genetics Analysis across computing platforms. *Molecular Biology and Evolution* 35: 1547–1549. <https://doi.org/10.1093/molbev/msy096>
- Lawson R, Slowinski JB, Crother BI, Burbrink FT (2005) Phylogeny of the Colubroidea (Serpentes): New evidence from mitochondrial and nuclear genes. *Molecular Phylogenetics and Evolution* 37: 581–601. <https://doi.org/10.1016/j.ympev.2005.07.016>
- Linnaeus C (1758) *Systema nature per regna tria naturæ, secundum classes, ordines, genera, species, cum characteribus, differentiis, synonymiis, locis*. Tomus I. Editio decima, reformata. Laurentii Salvii, Holmiae [= Stockholm], 824 pp. <https://doi.org/10.5962/bhl.title.542>

- Loebmann D, Haddad CFB (2010) Amphibians and reptiles from a highly diverse area of the Caatinga domain: Composition and conservation implications. *Biota Neotropica* 10: 227–256. <https://doi.org/10.1590/S1676-06032010000300026>
- Maddison WP, Maddison DR (2016) Mesquite: A modular system for evolutionary analysis. Version 3.10. Available from: <http://mesquite-project.org>.
- Mângia S, Koroiva R, Nunes PMS, Roberto IJ, Ávila RW, Sant'anna AC, Santana DJ, Garda AA (2018) A New Species of *Proceratophrys* (Amphibia: Anura: Odontophrynidae) from the Araripe Plateau, Ceará State, Northeastern Brazil. *Herpetologica* 74: 255–268. <https://doi.org/10.1655/Herpetologica-D-16-00084.1>
- Manly BFJ (2000) *Multivariate Statistical Methods*. 2nd Edition. Chapman and Hall/CRC, Boca Raton, 224 pp.
- Matioli SR, Fernandes FMC (2012) *Biologia Molecular e Evolução*. Holos, Ribeirão Preto, 256 pp.
- McDonald JH (2014) *Handbook of Biological Statistics*. 3rd Edition. Sparky House Publishing, Baltimore, 299 pp.
- Merrem B (1820) Versuch eines Systems der Amphibien (Tentamen Systematis Amphibiorum). Johann Christian Krieger, Marburg, 191 pp.
- Miller MA, Pfeiffer W, Schwartz T (2010) Creating the CIPRES Science Gateway for inference of large phylogenetic trees. In: Gateway Computing Environments Workshop (GCE). IEEE, New Orleans, 1–8. <https://doi.org/10.1109/GCE.2010.5676129>
- Morel E (1967) *Vendaal da Liberdade*. 2nd Edition. Editora Civilização Brasileira, Rio de Janeiro, 209 pp.
- Moura MR, Costa HC, Abegg AD, Alaminos E, Angarita-Sierra T, Azevedo WS, Cabral H, Carvalho P, Cechin S, Citeli N, Dourado ACM, Duarte AVF, França FGR, Freire EMX, Garcia PCA, Mol R, Montero R, Moraes-Da-Silva A, Passos DC, Passos P, Perez R, Pleguezuelos JM, Prado P, Prudente ALC, Sales RFD, Santana DJ, Santos LC, Silva VTC, Sudré V, Torres-Carvajal O, Torres-Ramirez JJ, Wallach V, Winck GR, Guedes JJM (2022) Unwrapping broken tails: Biological and environmental correlates of predation pressure in limbless reptiles. *Journal of Animal Ecology* 92: 324–337. <https://doi.org/10.1111/1365-2656.13793>
- Muscarella R, Galante PJ, Soley-Guardia M, Boria RA, Kass JM, Uriarte M, Anderson RP (2014) ENMeval: An R package for conducting spatially independent evaluations and estimating optimal model complexity for Maxent ecological niche models. *Methods in Ecology and Evolution* 5: 1198–1205. <https://doi.org/10.1111/2041-210x.12261>
- Naimi B, Hamm NAS, Groen TA, Skidmore AK, Toxopeus AG (2014) Where is positional uncertainty a problem for species distribution modelling? *Ecography* 37: 191–203. <https://doi.org/10.1111/j.1600-0587.2013.00205.x>
- Nascimento JLJ (2018) Comunidades quilombolas rurais do Ceará: Invisibilidade e desafios no processo de titulação dos territórios de maioria negra. In: Silva SPS, dos Santos MP, Junior HC, Bié EF, da Silva MS (Eds) *Afroceará Quilombola*. Editora Fi, Porto Alegre, 121–137.
- Nunes PMS, Fouquet A, Curcio FF, Kok PJR, Rodrigues MT (2012) Cryptic species in *Iphisa elegans* Gray, 1851 (Squamata: Gymnophthalmidae) revealed by hemipenial morphology and molecular data. *Zoological Journal of the Linnean Society* 166: 361–376. <https://doi.org/10.1111/j.1096-3642.2012.00846.x>
- Orejas-Miranda BR (1958) Dos especies de ofidios nuevos para el Uruguay. *Comunicaciones Zoológicas del Museo de Historia Natural de Montevideo* 79: 1–6.
- Padial JM, Miralles A, De la Riva I, Vences M (2010) The integrative future of taxonomy. *Frontiers in Zoology* 7: 1–14. <https://doi.org/10.1186/1742-9994-7-16>
- Palumbi S, Martin A, Romano S, McMillan WO, Stice L, Grabowski G (2002) The simple fool's guide to PCR, version 2.0. Department of Zoology and Kewalo Marine Laboratory, University of Hawaii, Honolulu, HI, 45 pp.
- Pante E, Schoelinc C, Puillandre N (2015) From integrative taxonomy to species description: One step beyond. *Systematic Biology* 64: 152–160. <https://doi.org/10.1093/sysbio/syu083>
- Passoni JC, Benozzati ML, Rodrigues MT (2008) Phylogeny, species limits, and biogeography of the Brazilian lizards of the genus *Eurolophosaurus* (Squamata: Tropiduridae) as inferred from mitochondrial DNA sequences. *Molecular Phylogenetics and Evolution* 46: 403–414. <https://doi.org/10.1016/j.ympev.2007.10.022>
- Passos P, Fernandes DS, Borges-Nojosa DM (2007) A new species of *Atractus* (Serpentes: Dipsadinae) from a relictual forest in northeastern Brazil. *Copeia* 2007: 788–797. [https://doi.org/10.1643/0045-8511\(2007\)7\[788:ansoas\]2.0.co;2](https://doi.org/10.1643/0045-8511(2007)7[788:ansoas]2.0.co;2)
- Passos P, Martins A, Pinto-Coelho D (2016) Population morphological variation and natural history of *Atractus potschi* (Serpentes: Dipsadidae) in Northeastern Brazil. *South American Journal of Herpetology* 11: 188–211. <https://doi.org/10.2994/SAJH-D-16-00034.1>
- Passos P, Melo-Sampaio PR, Ramos LO, Grazziotin FG, Fouquet A, Torres-Carvajal O (2022) When the tail shakes the snake: Phylogenetic affinities and morphology of *Atractus badius* (Serpentes: Dipsadidae), reveals some current pitfalls on the snake's genomic age. *Anais da Academia Brasileira de Ciências* 94: e20191254. <https://doi.org/10.1590/0001-376520220191254>
- Paynter Jr. RA, Traylor Jr. MA (1991) *Ornithological Gazetteer of Brazil*. Bird Department, Museum of Comparative Zoology, Harvard University, Cambridge, MA, viii + 789 pp. (2 volumes) + 2 maps.
- Peres EA, Pinto-Da-Rocha R, Lohmann LG, Michelangeli FA, Miyaki CY, Carnaval AC (2020) Patterns of species and lineage diversity in the Atlantic Rainforest of Brazil. In: Rull V, Carnaval AC (Eds) *Neotropical Diversification: Patterns and Processes*. Springer, Cham and Heidelberg, 415–447. https://doi.org/10.1007/978-3-030-31167-4_16
- Pesantes OS (1994) A method for preparing the hemipenis of preserved snakes. *Journal of Herpetology* 28: 93–95.
- Peters JA, Orejas-Miranda B (1970) *Catalogue of the Neotropical Squamata*. Part I. Snakes. United States National Museum Bulletin 297: 1–347.
- Phillips SJ, Anderson RP, Schapire RE (2006) Maximum entropy modeling of species geographic distributions. *Ecological Modelling* 190: 231–259. <https://doi.org/10.1016/j.ecolmodel.2005.03.026>
- Pinto RR, Marques OAV, Fernandes R (2010) Reproductive biology of two sympatric colubrid snakes, *Chironius flavolineatus* and *Chironius quadricarinatus*, from the Brazilian Cerrado domain. *Amphibia-Reptilia* 31: 463–473. <https://doi.org/10.1163/0173537-10X518423>
- Posada D (2008) jModelTest: Phylogenetic model averaging. *Molecular Biology and Evolution* 25: 1253–1256. <https://doi.org/10.1093/molbev/msn083>
- Pyron RA, Burbrink FT, Colli GR, de Oca ANM, Vitt LJ, Kuczynski CA, Wiens JJ (2011) The phylogeny of advanced snakes (Colubroidea), with discovery of a new subfamily and comparison of support methods for likelihood trees. *Molecular Phylogenetics and Evolution* 58: 329–342. <https://doi.org/10.1016/j.ympev.2010.11.006>

- QGIS Development Team (2023) QGIS Geographic Information System. Open Source Geospatial Foundation Project. Available from: <http://qgis.osgeo.org>.
- R Core Team (2022) R: A language and environment for statistical computing. R Foundation for Statistical Computing, Vienna, Austria. Available at: <http://www.R-project.org>.
- Rambaut A, Drummond AJ (2007) Tracer, version 1.4. Available at: <http://beast.bio.ed.ac.uk/tracer>.
- Recoder RS, Rodrigues MT (2020) Diversification processes in lizards and snakes from the middle São Francisco River Dune Region, Brazil. In: Rull V, Carnaval AC (Eds) Neotropical Diversification: Patterns and Processes. Springer, Cham and Heidelberg, 713–740. https://doi.org/10.1007/978-3-030-31167-4_26
- Roberto IJ, Brito L, Thomé MTC (2014) A new species of *Rhinella* (Anura: Bufonidae) from northeastern Brazil. South American Journal of Herpetology 9: 190–199. <https://doi.org/10.2994/SAJH-D-13-00028.1>
- Roberto IJ, Loebmann D (2016) Composition, distribution patterns, and conservation priority areas for the herpetofauna of the state of Ceará, northeastern Brazil. Salamandra 52: 134–152.
- Roberto IJ, Loebmann D, Lyra ML, Haddad CFB, Ávila RW (2022) A new species of *Pristimantis* Jiménez de la Espada, 1870 (Anura: Strabomantidae) from the “Brejões de Altitude” in Northeast Brazil. Zootaxa 5100: 521–540. <https://doi.org/10.11646/zootaxa.5100.4.4>
- Rodrigues MT (1996) Lizards, snakes, and amphisbaenians from the Quaternary sand dunes of the middle Rio São Francisco, Bahia, Brazil. Journal of Herpetology 30: 513–523. <https://doi.org/10.2307/1565694>
- Ronquist F, Huelsenbeck JP (2003) MrBayes 3: Bayesian phylogenetic inference under mixed models. Bioinformatics 19: 1572–1574. <https://doi.org/10.1093/bioinformatics/btg180>
- Sabaj MH (2020) Codes for Natural History Collections in Ichthyology and Herpetology. Copeia 108: 593–669. <https://doi.org/10.1643/ASIHCODONS2020>
- Schlegel H (1837) Essai sur la physionomie des serpens. Partie descriptive: Volume 2. M.H. Schonekat, Amsterdam, xv + 606 pp. + 21 plates. <https://doi.org/10.5962/bhl.title.4273>
- Schoener TW (1968) The *Anolis* lizards of Bimini: Resource partitioning in a complex fauna. Ecology 49: 704–726. <https://doi.org/10.2307/1935534>
- Silveira MHB, Mascarenhas R, Cardoso D, Batalha-Filho H (2019) Pleistocene climatic instability drove the historical distribution of forest islands in the northeastern Brazilian Atlantic Forest. Palaeogeography, Palaeoclimatology, Palaeoecology 527: 67–76. <https://doi.org/10.1016/j.palaeo.2019.04.028>
- Sneath RR, Sokal PHA (1973) Numerical Taxonomy. W.H. Freeman, San Francisco, CA, 573 pp.
- StatSoft Inc. (2011) STATISTICA (Data Analysis Software System), version 10. www.statsoft.com.
- Subbaraman N (2020) Thousands of scientists worldwide to go on strike for black lives. Nature. <https://doi.org/10.1038/d41586-020-01721-x>
- Sudré V, Curcio FF, Nunes PMS, Pellegrino KCM, Rodrigues MT (2017) Who is the red-bearded snake, anyway? Clarifying the taxonomic status of *Chironius pyrhopogon* (Wied, 1824) (Serpentes: Colubridae). Zootaxa 4319: 143–156. <https://doi.org/10.11646/zootaxa.4319.1.7>
- Tabarelli M, Silva JMC (2003) Áreas e ações prioritárias para a conservação da biodiversidade da Caatinga. In: Leal IR, Tabarelli M, Silva JMC (Eds) Ecologia e Conservação da Caatinga. Ed. Universitária da UFPE, Recife, 777–796.
- Thomé MTC, Carstens BC, Rodrigues MT, Alexandrino J, Haddad CFB (2021) Genomic data from the Brazilian sibilator frog reveal contrasting pleistocene dynamics and regionalism in two South American dry biomes. Journal of Biogeography 48: 1112–1123. <https://doi.org/10.1111/jbi.14064>
- Thompson JD, Higgins DG, Gibson TJ (1994) CLUSTAL W: Improving the sensitivity of progressive sequence alignment through sequence weighting, position-specific gap penalties and weight matrix choice. Nucleic Acids Research 22: 4673–4680. <https://doi.org/10.1093/nar/22.22.4673>
- Torres-Carvajal O, Echevarría LY, Lobos SE, Venegas PJ, Kok PJR (2019a) Phylogeny, diversity and biogeography of Neotropical sipo snakes (Serpentes, Colubridae, *Chironius*). Molecular Phylogenetics and Evolution 130: 315–329. <https://doi.org/10.1016/j.ympev.2018.10.022>
- Torres-Carvajal O, Koch C, Valencia JH, Venegas PJ, Echevarría LY (2019b) Morphology and distribution of the South American snake *Chironius leucometapus* (Serpentes: Colubridae). Phyllomedusa 18: 241–254. <https://doi.org/10.11606/issn.2316-9079.v18i2p241-254>
- Uetz P, Freed P, Aguilar R, Reyes F, Hošek J (2023) The Reptile Database. Available at: <http://www.reptile-database.org> (accessed on August 11, 2023).
- Uzzell T (1973) A revision of lizards of the genus *Prinodactylus*, with a new genus for *P. leucostictus* and notes on the genus *Euspondylus* (Sauria, Teiidae). Postilla 159: 1–67.
- Vanzolini PE (1981) A quasi-historical approach to the natural history of the differentiation of reptiles in tropical geographic isolates. Papéis Avulsos de Zoologia 34: 189–204.
- Vanzolini PE, Myers CW (2015) The herpetological collection of Maximilian, Prince of Wied (1782–1867), with special reference to Brazilian materials. Bulletin of the American Museum of Natural History 395: 1–155. <https://doi.org/10.1206/910.1>
- Vences M, Thomas M, van der Meijden A, Chiari Y, Vieites DR (2005) Comparative performance of the 16S rRNA gene in DNA barcoding of amphibians. Frontiers in Zoology 2: 5. <https://doi.org/10.1186/1742-9994-2-5>
- Vidal N, Kindl SG, Wong A, Hedges SB (2000) Phylogenetic relationships of xenodontine snakes inferred from 12S and 16S ribosomal RNA sequences. Molecular Phylogenetics and Evolution 14: 389–402. <https://doi.org/10.1006/mpev.1999.0717>
- Wagler JG (1830) Natürliches System der Amphibien, mit vorangehender Classification der Säugethiere und Vögel. Ein Beitrag zur vergleichenden Zoologie. J.G. Cotta'sche Buchhandlung, München, Stuttgart and Tübingen, vi + 354 pp. <https://doi.org/10.5962/bhl.title.58730>
- Warren DL, Glor RE, Turelli M (2008) Environmental niche equivalency versus conservatism: Quantitative approaches to niche evolution. Evolution 62: 2868–2883. <https://doi.org/10.1111/j.1558-5646.2008.00482.x>
- Wied M (1820) Reise nach Brasilien in den Jahren 1815 bis 1817. Volume 1. H. L. Brönnner, Frankfurt am Main, xxxiv + 385 pp.
- Wied M (1824) Abbildungen zur Naturgeschichte Brasiliens. Volume 8. Verlag des Großherzoglich Sächsisch Priviligerten Landes-Industrie-Comptoirs, Weimar, 90 plates.
- Wied M (1825) Beiträge zur Naturgeschichte von Brasilien. Volume 1. Verlag des Großherzoglich Sächsisch Priviligerten Landes-Industrie-Comptoirs, Weimar, xxii + 614 pp. + 1 plate.

- Wiens JJ, Servedio MR (2000) Species delimitation in systematics: Inferring diagnostic differences between species. *Proceedings of the Royal Society B* 267: 631–636. <https://doi.org/10.1098/rspb.2000.1049>
- Wiens JJ, Graham CH (2005) Niche conservatism: Integrating Evolution, Ecology, and Conservation Biology. *Annual Review of Ecology, Evolution, and Systematics* 36: 519–539. <https://doi.org/10.1146/annurev.ecolsys.36.102803.095431>
- Williams JD, Francini F (1991) A checklist of the Argentine snakes. *Bollettino del Museo Regionale di Scienze Naturali di Torino* 9: 55–90.
- Willis EO (2003) Bird records in the southern Neotropics: On the need to critically check specimens, literature citations and field observations. *Ornitologia Neotropical* 14: 549–552.
- Zaher H (1999) Hemipenial morphology of the South American xenodontine snakes, with a proposal for a monophyletic Xenodontinae and a reappraisal of colubroid hemipenes. *Bulletin of the American Museum of Natural History* 240: 1–168.
- Zar JH (2010) *Biostatistical Analysis*. 5th Edition. Prentice-Hall Pearson, Upper Saddle River, NJ, 944 pp.

Supplementary Material 1

Figure S1

Authors: Sudré V, Andrade-Junior A, Folly M, Azevedo JAR, Ávila RW, Curcio FF, Nunes PMS, Passos P (2024)

Data type: .pdf

Explanation note: Phylogenetic relationships of the *Chironius bicarinatus* complex estimated under Bayesian Inference based on four molecular markers (12S, 16S, ND4, c-mos) concatenated from a final matrix of 2,166 bp.

Copyright notice: This dataset is made available under the Open Database License (<http://opendatacommons.org/licenses/odbl/1.0>). The Open Database License (ODbL) is a license agreement intended to allow users to freely share, modify, and use this dataset while maintaining this same freedom for others, provided that the original source and author(s) are credited.

Link: <https://doi.org/vz.74.e106238.suppl1>

Supplementary Material 2

Table S1

Authors: Sudré V, Andrade-Junior A, Folly M, Azevedo JAR, Ávila RW, Curcio FF, Nunes PMS, Passos P (2024)

Data type: .xlsx

Explanation note: Genetic differences among and within species of *Chironius* calculated from the uncorrected pairwise genetic distances (p-distance; %) for sequences of 16S rRNA.

Copyright notice: This dataset is made available under the Open Database License (<http://opendatacommons.org/licenses/odbl/1.0>). The Open Database License (ODbL) is a license agreement intended to allow users to freely share, modify, and use this dataset while maintaining this same freedom for others, provided that the original source and author(s) are credited.

Link: <https://doi.org/vz.74.e106238.suppl2>

Supplementary Material 3

Table S2

Authors: Sudré V, Andrade-Junior A, Folly M, Azevedo JAR, Ávila RW, Curcio FF, Nunes PMS, Passos P (2024)

Data type: .xlsx

Explanation note: Morphological data of examined specimens of the *Chironius bicarinatus* complex.

Copyright notice: This dataset is made available under the Open Database License (<http://opendatacommons.org/licenses/odbl/1.0>). The Open Database License (ODbL) is a license agreement intended to allow users to freely share, modify, and use this dataset while maintaining this same freedom for others, provided that the original source and author(s) are credited.

Link: <https://doi.org/vz.74.e106238.suppl3>

Supplementary Material 4

Tables S3–S6

Authors: Sudré V, Andrade-Junior A, Folly M, Azevedo JAR, Ávila RW, Curcio FF, Nunes PMS, Passos P (2024)

Data type: .docx

Explanation notes: **Table S3.** Selected models based on delta-AICc lower than 10 for model projection of *Chironius bicarinatus* and respective parameters: Feature Classes (FC), Regularization Multipliers (RM). — **Table S4.** Variable importance results for *Chironius bicarinatus* derived from the MaxEnt model. Notice that we preselected variables with low VIF prior the modeling. — **Table S5.** Selected models based on delta-AICc lower than 10 for model projection of *Chironius gouveai* and respective parameters: Feature Classes (FC), Regularization Multipliers (RM). — **Table S6.** Variable importance results for *Chironius gouveai* derived from the MaxEnt model. Notice that we preselected variables with low VIF prior the modeling.

Copyright notice: This dataset is made available under the Open Database License (<http://opendatacommons.org/licenses/odbl/1.0>). The Open Database License (ODbL) is a license agreement intended to allow users to freely share, modify, and use this dataset while maintaining this same freedom for others, provided that the original source and author(s) are credited.

Link: <https://doi.org/vz.74.e106238.suppl4>

Supplementary Material 5

Appendix 1

Authors: Sudré V, Andrade-Junior A, Folly M, Azevedo JAR, Ávila RW, Curcio FF, Nunes PMS, Passos P (2024)

Data type: .pdf

Explanation notes: Examined specimens (n = 949) with their respective localities.

Copyright notice: This dataset is made available under the Open Database License (<http://opendatacommons.org/licenses/odbl/1.0>). The Open Database License (ODbL) is a license agreement intended to allow users to freely share, modify, and use this dataset while maintaining this same freedom for others, provided that the original source and author(s) are credited.

Link: <https://doi.org/vz.74.e106238.suppl5>

Supplementary Material 6

Appendix 2

Authors: Sudré V, Andrade-Junior A, Folly M, Azevedo JAR, Ávila RW, Curcio FF, Nunes PMS, Passos P (2024)

Data type: .pdf

Explanation note: Photographic material of specimens while alive obtained from iNaturalist observations.

Copyright notice: This dataset is made available under the Open Database License (<http://opendatacommons.org/licenses/odbl/1.0>). The Open Database License (ODbL) is a license agreement intended to allow users to freely share, modify, and use this dataset while maintaining this same freedom for others, provided that the original source and author(s) are credited.

Link: <https://doi.org/vz.74.e106238.suppl6>

Supplementary Material 7

Appendix 3

Authors: Sudré V, Andrade-Junior A, Folly M, Azevedo JAR, Ávila RW, Curcio FF, Nunes PMS, Passos P (2024)

Data type: .pdf

Explanation notes: GenBank accession numbers of species of *Chironius* and outgroup taxa included in the molecular analysis. Specimens in bold refer to the new sequences generated in this study.

Copyright notice: This dataset is made available under the Open Database License (<http://opendatacommons.org/licenses/odbl/1.0>). The Open Database License (ODbL) is a license agreement intended to allow users to freely share, modify, and use this dataset while maintaining this same freedom for others, provided that the original source and author(s) are credited.

Link: <https://doi.org/vz.74.e106238.suppl7>

Supplementary Material 8

Appendix 4

Authors: Sudré V, Andrade-Junior A, Folly M, Azevedo JAR, Ávila RW, Curcio FF, Nunes PMS, Passos P (2024)

Data type: .pdf

Explanation note: Primer sequences and PCR protocols.

Copyright notice: This dataset is made available under the Open Database License (<http://opendatacommons.org/licenses/odbl/1.0>). The Open Database License (ODbL) is a license agreement intended to allow users to freely share, modify, and use this dataset while maintaining this same freedom for others, provided that the original source and author(s) are credited.

Link: <https://doi.org/vz.74.e106238.suppl8>